THE LOW LEVEL OF DEBRIS DISK ACTIVITY AT THE TIME OF THE LATE HEAVY BOMBARDMENT: A *SPITZER* STUDY OF PRAESEPE

A. Gáspár[1], G. H. Rieke[1], K. Y. L. Su[1], Z. Balog[1], D. Trilling[1,2], J. Muzzerole[1,3], D. Apai[1,3], and Kelly, B. C.[4,5]

Draft version March 24, 2009

ABSTRACT

We present 24 μm photometry of the intermediate-age open cluster Praesepe. We assemble a catalog of 193 probable cluster members that are detected in optical databases, the Two Micron All Sky Survey (2MASS), and at 24 μm, within an area of $\sim$ 2.47 square degrees. Mid-IR excesses indicating debris disks are found for one early-type and for three solar-type stars. Corrections for sampling statistics yield a 24 μm excess fraction (debris disk fraction) of $6.5 \pm 4.1\%$ for luminous and $1.9 \pm 1.2\%$ for solar-type stars. The incidence of excesses is in agreement with the decay trend of debris disks as a function of age observed for other cluster and field stars. The values also agree with those for older stars, indicating that debris generation in the zones that emit at 24 μm falls to the older 1-10 Gyr field star sample value by roughly 750 Myr.

We discuss our results in the context of previous observations of excess fractions for early- and solar-type stars. We show that solar-type stars lose their debris disk 24 μm excesses on a shorter timescale than early-type stars. Simplistic Monte Carlo models suggest that, during the first Gyr of their evolution, up to 15-30% of solar-type stars might undergo an orbital realignment of giant planets such as the one thought to have led to the Late Heavy Bombardment, if the length of the bombardment episode is similar to the one thought to have happened in our Solar System.

In the Appendix, we determine the cluster's parameters via boostrap Monte Carlo isochrone fitting, yielding an age of 757 Myr ($\pm$ 36 Myr at 1σ confidence) and a distance of 179 pc ($\pm$ 2 pc at 1σ confidence), not allowing for systematic errors.

Subject headings: infrared: stars – open clusters and associations: individual (Praesepe, M44, NGC 2632, Beehive) – stars: evolution – stars: circumstellar matter – planetary systems: formation

1. INTRODUCTION

Stars generally form with an accompanying circumstellar disk. Planets can grow from this primordial disk over a few to a few tens of Myr. The *Infrared Astronomy Satellite* (*IRAS*) detected infrared excess emission from disks around stars with ages much older than the clearing timescales of protoplanetary circumstellar disks (Aumann et al. 1984). These excesses arise from second-generation "debris disks" that are the results of collisional cascades initiated by impacts between planetesimals and of cometary activity (Backman & Paresce 1993). The micron-sized dust grains in debris disks are heated by the central star(s) and reradiate the received energy at mid-infrared wavelengths. Studying this infrared emission lets us probe the frequency of formation of planetary systems and to track their evolution. For example, some of the relatively prominent disks may be analogs to that in the Solar System at the epoch of Late Heavy Bombardment (LHB; e.g. Gomes et al. 2005; Strom et al. 2005).

IRAS and *Infrared Space Observatory* (*ISO*) observations of debris disks suggest that the excess rate steadily declines with stellar age, indicative of stars

losing these disks within a few hundred million years (Habing et al. 2001; Spangler et al. 2001). A theoretical model that involved delayed stirring was developed by Dominik & Decin (2003) to explain this phenomenon; however, a uniform evolutionary model could not be derived. There were a number of reasons. The sensitivity of these instruments was often inadequate for observations down to the photospheric levels. The large beam sizes also occasionally confused the excesses with background objects and/or the galactic cirrus. The Multiband Imaging Photometer for *Spitzer* (MIPS; Rieke et al. 2004) on the *Spitzer Space Telescope* has improved sensitivity and resolution in the mid-infrared and with it astronomers have been able to carry out more detailed statistical studies of debris disks at a wide range of stellar ages and spectral types.

Rieke et al. (2005) observed a large sample of nearby A-type field stars with *Spitzer*, which combined with existing *IRAS* and *ISO* data definitively demonstrated that the frequency of debris disk excesses declines with age and that the disk properties vary at all ages. Even by probing excesses down to 25% above the photospheric level, Rieke et al. (2005) found that some stars at ages of only 10-20 Myr do not show any signs of excess. These results were confirmed by Su et al. (2006). This behavior implies a very fast clearing mechanism for disks around some of these stars, or perhaps that they form with only very low mass disks. The models of Wyatt et al. (2007) provided a first-order explanation in terms of a steady state evolution of the debris disks from a broad distribution of initial masses.

Electronic address: agaspar@as.arizona.edu

[1] Steward Observatory, University of Arizona, Tucson, AZ 85721
[2] Department of Physics and Astronomy, Northern Arizona University, Flagstaff, AZ 86011
[3] Space Telescope Science Division of ESA, STScI, 3700 San Martin Drive, Baltimore, MD 21218
[4] Harvard-Smithsonian Center for Astrophysics, 60 Garden St, Cambridge, MA 02138
[5] Hubble Fellow

An important question for habitable planet search/evolution is whether the same processes occur for FGK-type stars. A number of surveys of solar-type stars have been conducted with *Spitzer*. The MIPS Guaranteed Time Observers (GTO) team has searched ∼ 200 field stars for excesses (Trilling et al. 2008), plus many hundreds of open cluster members (e.g., Gorlova et al. 2006, 2007; Siegler et al. 2007). The legacy survey by the Formation and Evolution of Planetary Systems (FEPS) group has examined 328 stars (both field and open cluster members)(Mamajek et al. 2004; Meyer et al. 2004, 2008; Stauffer et al. 2005; Kim et al. 2005; Silverstone et al. 2006).

Trilling et al. (2008) showed that solar-type stars of age older than 1 Gyr have excess emission at 70 μm ∼ 16% of the time. Excesses at this wavelength are expected to arise from Kuiper-Belt-like planetesimal regions, but with masses 10-100 times greater. Meyer et al. (2008) find that 8.5-19% of solar-type stars at ages < 300 Myr have debris disks detectable at 24 μm and that this number gradually goes down to < 4% at older ages, augmenting work by Gorlova et al. (2006), Siegler et al. (2007) and Trilling et al. (2008). Excesses at this wavelength around solar-type stars probe the 1-40 AU range, the asteroidal and planetary region in the Solar System.

The ideal laboratories to determine the stellar disk fractions with good number statistics are open clusters and associations. To investigate the fraction of solar-type excess stars, the observations have to be able to detect the photospheres of the non-excess stars. The range of distances to suitable clusters compromises the uniformity of the results. The survey of h and χ Persei (Currie et al. 2008) could only determine the early-type star excess fraction, while that of NGC 2547 (Young et al. 2004; Gorlova et al. 2007) could only detect photospheres down to early G due to similar limits. The observations in M47 (Gorlova et al. 2004) also yielded values to early G spectral type stars. The investigations of IC 2391 (Siegler et al. 2007) and the Pleiades (Gorlova et al. 2006) gave insights on debris disk evolution down as far as K spectral-type stars.

To study further the fraction of debris disks around solar-mass stars, we have observed the nearby Praesepe (M44, NGC 2632, Beehive) open cluster. Our observations, along with those of Cieza et al. (2008) on the Hyades cluster, fill the gap in previous work on debris disk fractions in the age range of 600-800 Myr. This range is of interest because it coincides with the LHB in the Solar System. The close proximity of the cluster (∼ 180 pc) and its large number of members ensured that good statistics would be achieved. Praesepe has been extensively studied by many groups (Klein Wassink 1927; Jones & Cudworth 1983; Jones & Stauffer 1991; Hambly et al. 1995; Wang et al. 1995; Kraus & Hillenbrand 2007), providing a nearly full membership list to our completeness limit of [24] ∼ 9 mag (the brightness of a G4 V spectral-type star at the distance of the cluster). The member stars have high proper motions (∼ 39 mas yr^{-1}), clearly distinguishing them from field stars.

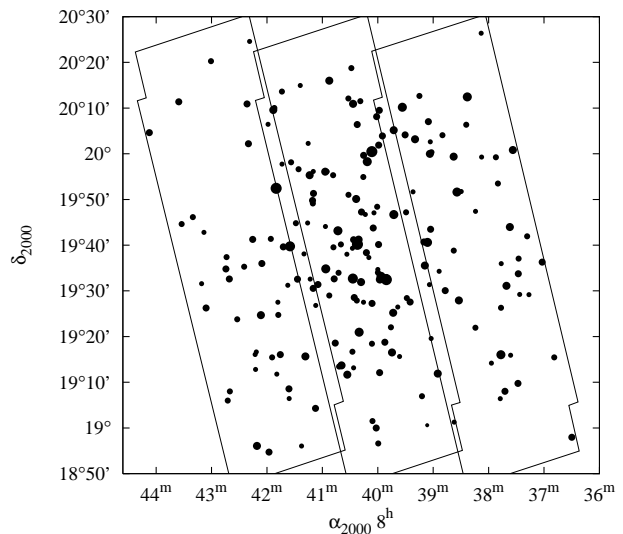## 2. OBSERVATIONS, DATA REDUCTION, AND PHOTOMETRY

FIG. 1.— The observed field, showing the areas covered by three scanmaps and the observed cluster member stars with sizes proportional to their brightness in [24].

We used MIPS to observe Praesepe as part of the GTO program PID 30429 (2007 May 30). The center part of the cluster ($8^h40^m21^s$, $19°38'40''$) was imaged using three scan maps (with 12 legs in a single scan map overlapping with half-array cross-scan). The map covers a field of ∼ 2.47 deg^2, as shown in Figure 1. We used medium scan mode, resulting in a total effective exposure time per pixel of 80 s (at 24 μm). All data were processed using the MIPS instrument team Data Analysis Tool (DAT, Gordon et al. 2005) as described by Engelbracht et al. (2007).

Although MIPS in scan-mode provides simultaneous data from all three detectors (at 24, 70 and 160 μm), we base our study on the 24 μm channel data only. The 70 and 160 μm detectors are insensitive to stellar photospheric emissions at the distance of Praesepe. In retrospect, the rarity of excesses in our survey is consistent with the lack of detections at the longer wavelengths.

The initial coordinate list for the 24 μm photometry was assembled with the daofind task under IRAF[6]. We later expanded this list by visually examining the images and manually adding all sources to the list that were missed by daofind. Our final list for photometry contained 1457 sources. To achieve high accuracy, we performed point-spread function (PSF)–fitting photometry. The calibration star HD 173398 was adopted as a PSF standard, with the final PSF constructed from 72 individual observations, kindly provided to us by C. Engelbracht. The standard IRAF tasks phot and allstar of the daophot package were used.

The observed field is free of nebulosity and stellar crowding, so we were able to use a large PSF radius of 112$''$, with fitting radius of 5.7$''$. The large PSF radius ensured us that the aperture correction was negligible. The instrumental number counts were converted to flux densities with the conversion 1.068 ×
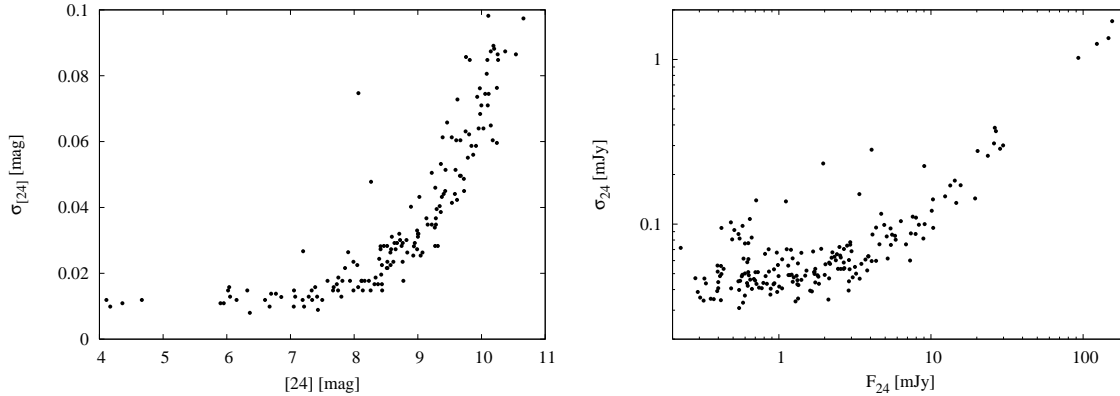
Fig. 2.— The error of the 24 μm photometry is plotted as a function of brightness for cluster member sources. The *left panel* shows the flux and its error on the magnitude scale, while the *right panel* shows them in mJy flux values. All points have less than 0.1 magnitude error and nearly all stars brighter than 9th magnitude have errors less than 0.04 magnitude.

10^{-3} mJy arcsec^{-2} MIPS_UNIT^{-1} (Engelbracht et al. 2007). We then translated these values to 24 μm magnitudes taking 7.17 Jy for the [24] magnitude zero point, which has error of $\pm$ 0.11 Jy (Rieke et al. 2008). We show the photometric error vs. brightness plots of our measurements in Figure 2. Almost all sources brighter than 9th magnitude ($\sim$ 1.8 mJy) have errors less than 0.04 mag ($\sim$ 0.07 mJy) and all sources remain below errors of 0.1 mag; the average error is $\sim$ 5%. As a check, we performed independent PSF photometry with `StarFinder` under IDL, obtaining photometry values within the errors of our IRAF photometry and with errors similar to the ones given by `daophot`.

3. CATALOG SURVEYS AND THE FINAL SAMPLE

We compiled a complete catalog for all sources in our field of view, including their optical, near infrared, and 24 μm data. We expanded this catalog with all known cluster members outside of our field of view (naturally without [24] data). This enabled us to plot a full cluster optical color-magnitude diagram (CMD), which we used to confirm the cluster's age and distance (see Appendix).

Optical data for the sources were obtained from the 5th data release of the Sloan Digital Sky Survey (SDSS), while 2MASS provided J, H, and K_S magnitudes. The SDSS photometry is generally unreliable for bright sources, the ones mostly detected in our MIPS survey. To ensure we had good photometry for these sources, we collected BV data (for 356 stars altogether) using the Webda database[7], providing an ensemble of data for high probability cluster members from various papers (Johnson 1952; Anthony-Twarog 1982; Dickens et al. 1968; Lutz & Lutz 1977; Upgren et al. 1979; Castelaz et al. 1991; Mermilliod et al. 1990; Weis 1981; Stauffer 1982; Andruk et al. 1995; Mendoza 1967; Oja 1985). The data downloaded from the Webda database cover the brightest magnitude range of the cluster, including stars avoided by modern CCD observations or where they are saturated. We converted the BV magnitudes to SDSS r and g values by averaging the conversion slopes of Jester et al. (2005); Jordi et al. (2006); Zhao & Newberg (2006) and Fukugita et al. (1996) and obtained

$$g = (0.607 \pm 0.016)(B - V)$$

[7] http://www.univie.ac.at/webda/

$$-(0.1153 \pm 0.0095) + V \qquad (1)$$
$$r = (-0.453 \pm 0.028)(B - V)$$
$$+(0.1006 \pm 0.0131) + V. \qquad (2)$$

Where our calculated r or g brightnesses for the Webda catalog members differed from the SDSS data by more than 0.5 magnitude, we replaced the SDSS data with the calculated one.

Cluster membership was determined by compiling all accessible databases. The largest membership lists are those of Wang et al. (1995) and Kraus & Hillenbrand (2007), which were supplemented by our Webda catalog search results. Wang et al. (1995) give a list of 924 stars, out of which we chose only 198 that are high probability members of the cluster according to the proper motion data in the paper. The list of Kraus & Hillenbrand (2007) is much more robust with 1130 stars, all of which have membership probability > 50%; 1010 of them have > 80% membership probability. The databases (SDSS, 2MASS, Webda, Wang et al. (1995), Kraus & Hillenbrand (2007)) were cross-correlated with a maximum matching radius of 3.6″. The closest member within this radius is matched as a pair and all others are added to the catalog as new sources. The program excluded pairing members from the same catalog. Our final cluster member list contains 1281 candidates, of which 493 were in our observed field.

After plotting the color-magnitude diagram and doing an initial isochrone fit on cluster members, we tested for bad photometry. We generated a list of all the member stars that were further from the isochrone sequence than 0.3 magnitude, examined all these stars for anomolies on SDSS images, and searched for BV magnitudes in Simbad. If the star was saturated or a calculated r, g magnitude differed from the SDSS r, g value by 0.5 magnitude or more (the same criteria as used before), we used the calculated value.

In Figure 3, we show how the selection criteria narrow the CMD, and where sources with different selection characteristics are distributed in the field. From the 1457 sources identified in our 24 μm survey, 201 were cataloged as cluster members by previous work. Of these, 193 also have data in the optical and near infrared. Our survey's completeness limit compared to 2MASS is at J = 10 mag ([24] $\sim$ 9 mag), as is shown in Figure 4. This limit corresponds to a G4 V star at the distance of Praesepe. The
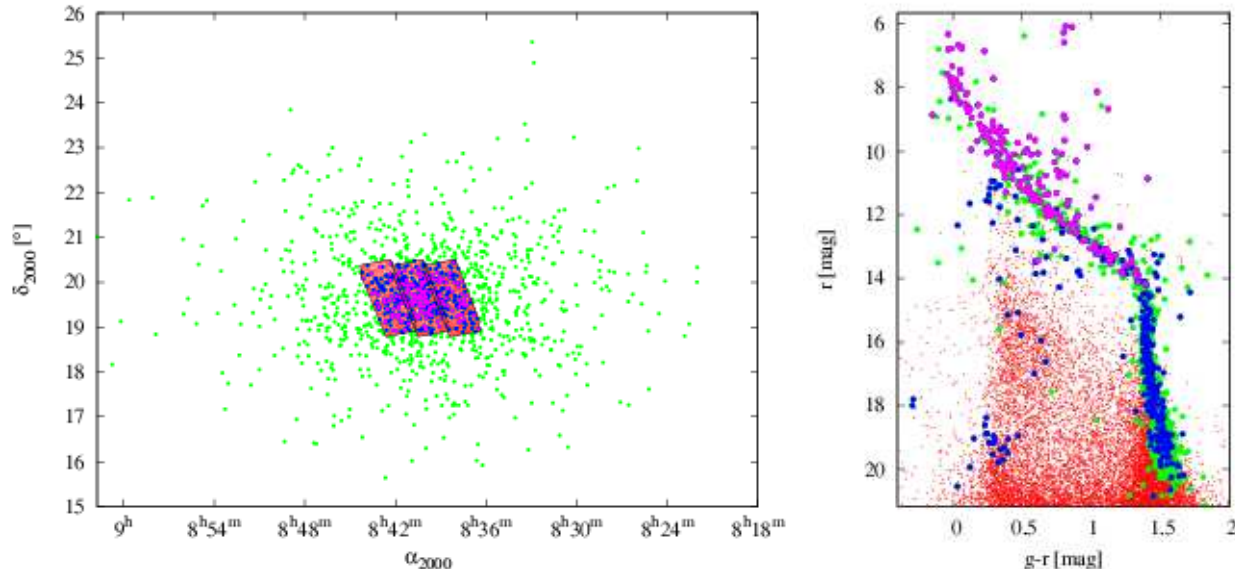
FIG. 3.— The spatial and CMD position of the selected sources. *Red dots:* The combined list for all sources in our observed field; *Green dots:* All cluster members outside our observed field; *Blue dots:* All cluster members in our observed field that could not be identified in our 24 μm survey; *Magenta dots:* All cluster members that were identified in our 24 μm survey.

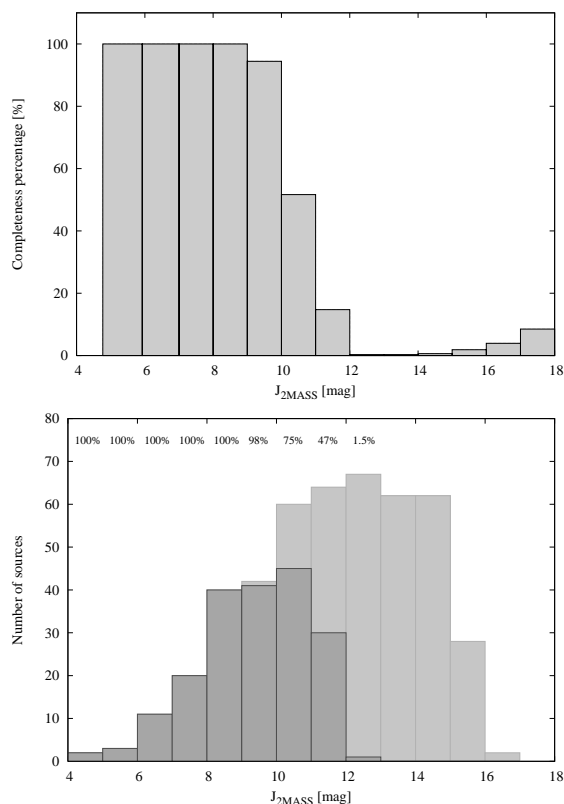FIG. 4.— *Left Panel:* The completeness limit of our survey is shown as a function of 2MASS J magnitude. We detect almost all sources brighter than 10th magnitude, corresponding to a ~ G4 V star. For sources fainter than 14th magnitude random associations begin to occur. *Right Panel:* The total number of cluster members within our field of view (light gray) and the number of members detected (dark gray) at [24] are shown as a function of J magnitude.

completeness limit for the cluster member sources is also shown in Figure 4. Between 10th and 11th magnitude in J we achieve 75% completeness for cluster members.

For our [24] magnitude values to be comparable to the 2MASS K_S photometry, we fitted a Gaussian to the binned number distribution of the K_S-[24] values of all member sources with r-K_S < 0.8 (~ A stars). We derived a general correction factor of -0.032±0.002 magnitude (~ 3%) for the [24] values. The Gaussian fits are shown in Figure 5. This same method has been used by Rieke et al. (2008) to obtain the average ratio of K_S to 24 μm flux densities. By optimizing the fit of our [24] data to the 2MASS K_S data, we eliminated any absolute calibration offsets. The average variance of the fitted gaussians is $\sigma = 0.047$ mag, consistent with our average [24] error value of ~ 0.05 mag.

We summarize our [24] photometry results for the 193 cluster members that were identified in all wavelength regions in Table 1. The first column of the table gives our designated number, while the coordinates are that of the 24 μm flux source. As a source/coordinate comparison we also list the 2MASS source associated with the 24 μm emission. The table contains the K_S adjusted [24] magnitude, the original flux values (in mJy) and the "best" r and g photometry value. Cluster membership probability is shown by either the proper motion of the source or by the Wang et al. (1995) catalog number of the source. Sources that are missing both values were listed as cluster members either in the Webda database or in Kraus & Hillenbrand (2007).

4. RESULTS

In this section we present our results on the debris disk fraction we observed in Praesepe and place it in context with previous results on the evolution of debris disks. There are two basic methods to detect 24 μm excess. The first is to use a color-color diagram, with one of the colors determining the stars' spectral type and the other being K_S-[24]. The r-K_S color is ideal to differentiate spectral types, while the K_S-[24] color depends only weakly on the spectral type of the star since both wavelengths fall on the Rayleigh-Jeans part of the spectral energy distri-
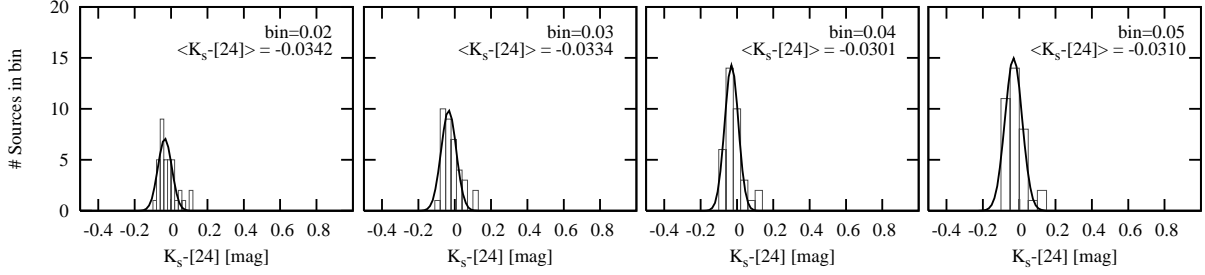
FIG. 5.— The panels show the Gaussian fits to the number distribution of A type stars, within certain K_S-[24] bins.

bution (SED) for all sources hotter than early M type ($T_{eff} > 3200$ K) (Gautier et al. 2007). For non-excess stars the K_S-[24] color should stay close to zero. Any excess measured in K_S-[24] is most likely caused by circumstellar material.

The second method is to fit the observed optical and near-infrared photometry with theoretical SEDs based on stellar photosphere models. Excesses are revealed if the 24 μm flux density is significantly greater than the predicted flux.

4.1. Color-color selection

We used the color-color diagram shown in Figure 6 as our primary method to identify sources as excess candidates. We plot all cluster members that have magnitude values in r, K_S, and [24], 193 sources altogether.

Gautier et al. (2007) show the trend of K_S-[24] photospheric color with spectral type for stars of low effective temperature. The empirical locus of stars on the color-color plot in Figure 6 was derived by fitting a curve to a sample of field stars (from Gautier et al. (2007) and Trilling et al. (2008)). We then converted the fitted V-K_S colors to r-K_S colors through conversion tables in Cox (2000) and Kraus & Hillenbrand (2007). Our final color-color curve for r-K_S vs. K_S-[24] for main-sequence (MS) stars is:

$$K_S - [24] = 3.01 \times 10^{-5}(r - K_S) + 0.0233(r - K_S)^2$$
$$+ 0.0072(r - K_S)^3 - 0.0015(r - K_S)^4. \quad (3)$$

In Figure 6, we plot this curve and the 3σ average confidence level for our photometry in [24] (~ 0.15 mag) (the errors of the curve itself are minor compared to the photometric errors). The majority of the stars ($> 86\%$) lie within this band. The errors plotted for the stars outside of our MS fitted curve are the 1σ errors in our [24] photometry. To use the K_S-[24] color as an excess diagnostic tool, one must make sure that the K_S magnitude is truly photospheric. We examined the J, H, and K_S fits to theoretical SEDs (Castelli & Kurucz 2003) and concluded that all K_S magnitudes are truly photospheric; the largest difference (from our debris disk candidate sample introduced later) is in the case of star 143, where the measured value is above the predicted SED value by 5.6%.

As Figure 6 shows, we have 7 stars in the "blue" region of the color-color plot, which we used to establish a selection rule to clean the excess region of the plot of possible spurious detections. We only accepted stars as true excess stars that: 1) lie at least $3\sigma_{24}$ (their own σ and not the average [24] error) from the trend line; 2) have [24]
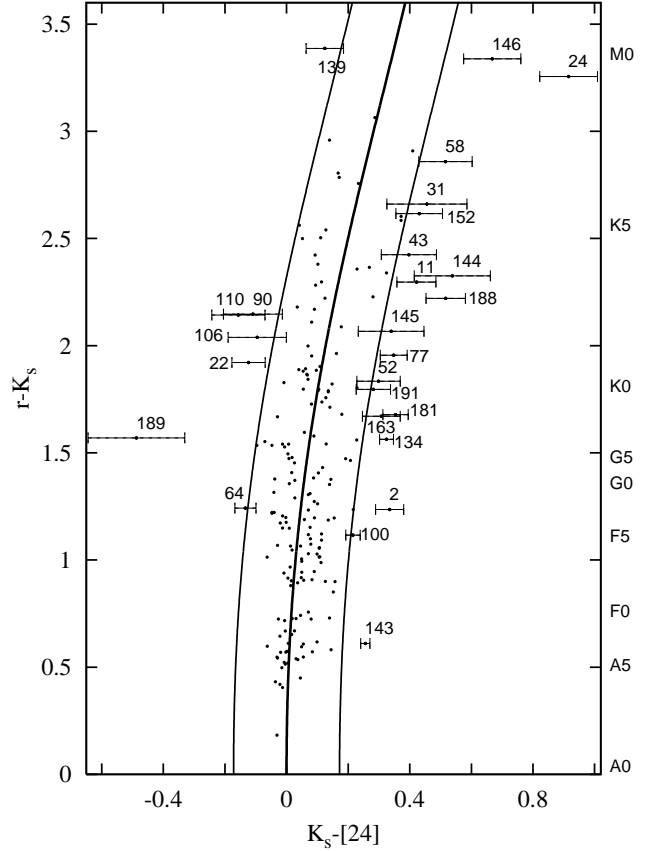
FIG. 6.— The color-color plot for the cluster members with photometric measurements in r, K_S, and [24]. The 1σ measurement error in [24] is plotted for stars that are outside of the trend curve. The nomenclature is from Table 1.

data at least $3\sigma_{24}$ from the best fitting SED solution also; and 3) are point sources on the images and have no noise anomalies. All stars in the "blue" region failed these criteria. From the 19 stars that lie in the excess ("red") region of the color-color diagram, fifteen were eliminated as debris disk candidates for the following reasons. Only 8 were $3\sigma_{24}$ from the trend line: 181, 143, 100, 77, 134, 188, 24, and 2 (in the nomenclature of Table 1 and Figure 6). Star 188 turned out to be contaminated by a minor planet, which was identified by comparing scanlegs separately. Stars 24 and 2 are resolved doubles on the higher resolution 2MASS and SDSS images, so we excluded them from our list.

Star 100 is contaminated by a faint background galaxy, which was visible as a faint nebulosity next to the star.

TABLE 2
The probabilities of chance alignments for our sources with background galaxies as a
function of [24] brightness.

[24] bin [mag]	N_* [#]	Flux [mJy]	Excess [mJy]	$N_{galaxies}$ [sr^{-1}]	P of at least n chance alignments				
					[0]*	[1]†	[2]†	[3]†	[4]†
4-5	4	125.900	16.245	2×10^4	99.99%	0.01%	$\sim$0%	$\sim$0%	$\sim$0%
5-6	2	50.122	6.467	7×10^4	99.98%	0.02%	$\sim$0%	-	-
6-7	11	19.954	2.575	4×10^5	99.54%	0.46%	$\sim$0%	$\sim$0%	$\sim$0%
7-8	26	7.944	1.025	1×10^6	97.46%	2.54%	0.04%	$\sim$0%	$\sim$0%
8-9	48	3.162	0.408	7×10^6	72.35%	27.65%	3.80%	0.01%	$\sim$0%
9-10	53	1.259	0.162	4×10^7	12.60%	87.40%	60.26%	31.93%	13.14%
10-11	48	0.501	0.065	8×10^7	2.47%	97.53%	87.34%	69.30%	47.06%
11-12	1	0.199	0.026	1×10^8	91.20%	8.80%	-	-	-

* The probability that none of the cluster member sources are chance aligned with a background
galaxy in the appropriate magnitude range.
† The probability that at least 1, 2, 3 or 4 cluster member sources are chance aligned with a
background galaxy in the appropriate magnitude range.

The probability for other sources of a 24 μm excess arising through a chance alignment with distant galaxies can be determined from galaxy counts (Papovich et al. 2004). Our $\sim$ 0.15 mag [24] excess criterion results in different flux values identified as excesses as a function of source brightness. We estimated the probability of chance alignments by dividing our sample into 1 magnitude bins and running a Monte Carlo code with the number of sources in the bin and the number of extragalactic sources corresponding to 0.15 magnitude excess value for the specific bin. The matching radius for the chance alignment was chosen to be $r = 3.6''$ and the code was ran to 10000 simulations per magnitude bin. We summarize the simulation numbers with the probabilities of at least n number of chance alignments in each bin in Table 2. The probability that star 143 with [24] = 7.04 mag is a chance alignment with a background galaxy is very low ($< 3\%$), so it is very likely to be a true debris disk star. The probability that at least two sources (star 100 and 134) are contaminated by a background galaxy in the 8-9 magnitude bin is also very low ($< 4\%$), and since star 100 is already contaminated, we classify star 134 as a real debris disk star also. The likelihood that stars 77 and 181 are contaminated within 3.6″ is high ($\sim$ 90%). However, there is no indication of any positional offset between K_S and [24], even at the 1″ level, so this likelihood is probably overestimated.

We determine stars 143 and 134 to be definite debris disk stars in Praesepe and list stars 77 and 181 as possible debris disk stars. We show these sources in Figure 7 and detail their properties in §4.4. Figure 7 shows that the fields are clean and that the sources are point-like. The PSFs were centered on the 24 μm sources with *IRAF*'s centroid algorithm. As Table 1 shows, the coordinate center of the excesses is closer than 1″ to the 2MASS coordinates for the debris disk candidates.

4.2. *The SED fit selection*

The 2MASS data are only useful in selecting debris disk candidates if the K_S magnitude is photospheric. Since the threshold of the K_S-[24] color above which a star is selected to be a debris disk candidate depends on the spectral type (the determination of which depends on correct r band photometry), we also fit the photometric data for all stars within the trend curves with model spectra to look for excess candidates. To be considered a debris disk candidate in this region required even stronger selection criteria then in the case of the "excess region stars." Stars were selected to be candidates from this region if their [24] photometry was at least $3\sigma_{24}$ from the fitted SED and if the star was $3\sigma_{24} + 10\%$ (0.1 mag) from the trend line in the color-color plot. The 10% is an allowance for systematic errors. None of the stars within the trend curves passed these criteria.

4.3. *Praesepe white dwarfs*

We also checked whether any of the known eleven Praesepe white dwarfs (Dobbie et al. 2006) were detected, indicating a possible white dwarf debris disk. WD 0837+199 showed a strong signal in [24]. The UKIRT Infrared Deep Sky Survey (UKIDSS) survey team (Sarah Casewell, private communication 2008) have found that this signal originates from a background galaxy a few arcseconds north of the WD.

4.4. *Debris Disk Candidates*

We discuss the four debris disk candidate stars in this section. None of these stars show extended emission (resolved disk), implying that the excess is confined to the radius of the MIPS beam of 6″ (Rieke et al. 2004), which is $\sim$ 1000 AU at the distance of Praesepe. This is consistent with the sizes of already resolved mid-IR debris disks (Stapelfeldt et al. 2004; Su et al. 2005, 2008; Backman et al. 2009). The best fitting SEDs of the debris disk candidate stars are plotted in Figure 8.

4.4.1. *Star #77*

This star was identified on three separate scanlegs, with no contamination by minor planets. It is rather faint with $m_V = 12.88$ mag. Its optical and NIR photometry was best fitted by the $T_{eff} = 5000$ K and $\log g = 4.5$ (K3 V) Kurucz model (Castelli & Kurucz 2003). Franciosini et al. (2003) used XMM-Newton to detect X-ray emission from it with a flux of $L_X = 1.67 \times 10^{28}$ erg s^{-1} in the *ROSAT* 0.1-2.4 keV band. They point out that the flux measured by ROSAT (Randich & Schmitt 1995) is a magnitude higher than theirs. The star is a cluster member cataloged in many papers (Wang et al. 1995; Klein Wassink 1927; Jones & Cudworth 1983).
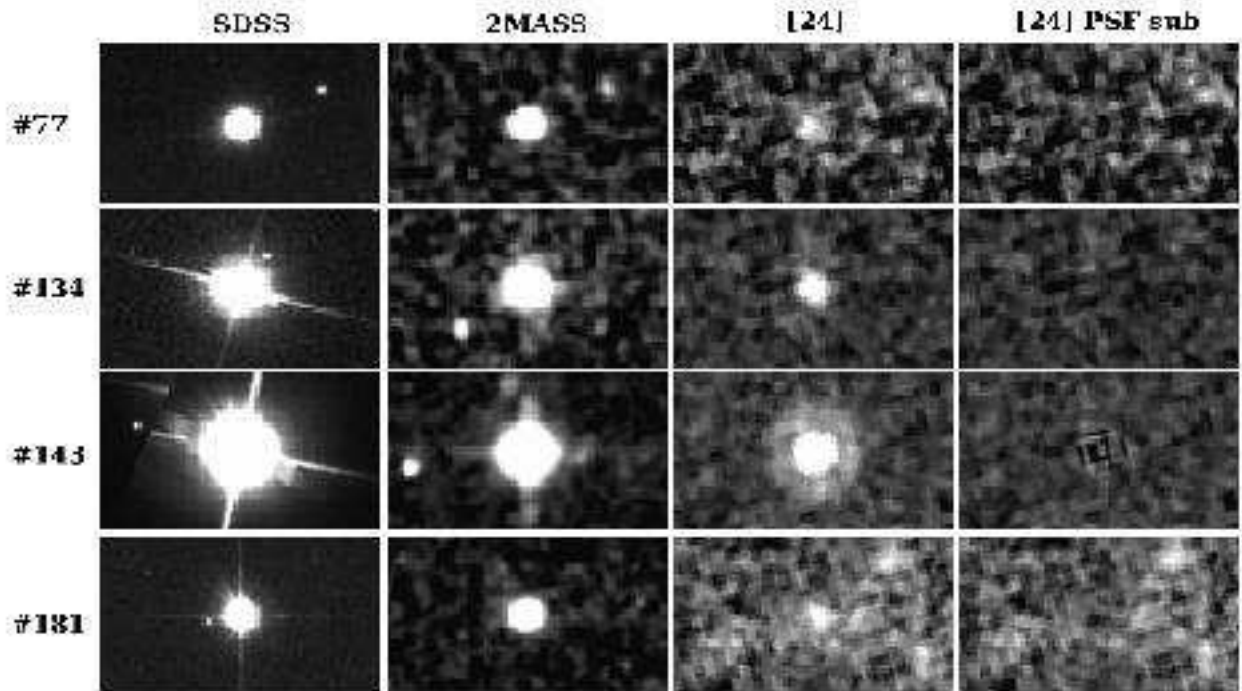
4.4.2. *Star #134*

Fig. 7.— SDSS, 2MASS, 24 micron, and 24 micron PSF subtracted images for stars 77, 134, 143, and 181. The fields of view (FOV) for the images are $69.9'' \times 37.97''$ and they have linear flux scaling.

Star #134 (WJJP 179, KW 367) is a bright cluster member, with $m_V = 10.71$ mag. It was imaged on two scanlegs with high S/N. Its optical and NIR photometry was best fitted by the $T_{eff} = 5500$ K and $\log g = 4.5$ (G8 V) Kurucz model (Castelli & Kurucz 2003) and we detect no extent to the stellar PSF core (Figure 7). North of it by $6''$, a fainter extended source is visible on both scanlegs. It has been found to be a triple system by Mermilliod et al. (1994) and the mass of the components was estimated by Halbwachs et al. (2003) using CORAVEL radial velocity measurements. The system consists of a wide pair, one of which is a spectroscopic binary with a period of 3.057 days. It is also a definite cluster member (Wang et al. 1995; Klein Wassink 1927; Jones & Cudworth 1983).

4.4.3. Star #143

This is the brightest of all debris disk stars we observed, with $m_V = 8.04$ mag. Its optical and NIR photometry was best fitted with a $T_{eff} = 7500$ K, $\log g = 5.0$ (A7 V) Kurucz model (Castelli & Kurucz 2003). The PSF subtraction was very clean, with no hint of any extended emission (Figure 7). The star was discovered to be a δ Scuti type of pulsating variable by Paparó & Kolláth (1990) (HI Cnc, HD 73890, BD+19 2078). It has been cataloged as a definite cluster member in many papers (Wang et al. 1995; Klein Wassink 1927; Jones & Cudworth 1983). With high-resolution imaging surveys, Mason et al. (1993) found it to be a single star.

4.4.4. Star #181

The star was identified on three separate scanlegs. The best fit to its photometry points was with a $T_{eff} = 5250$ K, $\log g = 4.5$ (K0 V) Kurucz model (Castelli & Kurucz 2003). It has been identified as a cluster member in many catalogs

(Wang et al. 1995; Hambly et al. 1995; Klein Wassink 1927; Jones & Stauffer 1991). It was not identified as a close binary star in the surveys of Bouvier et al. (2001) and Mermilliod & Mayor (1999). No extended emission is seen in our PSF subtracted image (Figure 7).

5. DISCUSSION

We have found 4 sources out of 193 in the spectral range from A0 to K3 showing excess at 24 μm. One of our sources (star 143) is an A7 type star (out of 29 early-type stars), while the remaining three are G8, K0, and K3 (out of 164 solar-type stars), based on their photometric colors and fitted SEDs. Although the probability of chance alignments with faint background galaxies within $3.6''$ are rather high for the K0 and K3 spectral-type sources, since the peaks of their emission are well within $1''$ of the 2MASS coordinates they are likely excess sources. However, our statistics are incomplete to their spectral limit. In our field of view there are 106 stars within F0 and G8 spectral-type, of which we detected 98, meaning we have an almost complete sample of sources within this spectral band. We use the excess fraction of 1/106 for the solar-type star sample.

The excesses found around early type stars (B8-A9) are usually dealt with separately in the literature from the ones found around solar-type stars (F0-K4), because the dominant grain removal processes in the debris disks may not be the same and the 24 μm excesses probe significantly different distances from the stars. These populations are also separated observationally, by the natural detection limits.

In the following sections we analyze our results in the context of previous debris disk fractions observed around early- and solar-type stars. The errors on our debris disk fractions are given by Bayesian statistics detailed in the following §5.1. We contrast the results for early- and solar-type stars in §5.2 and §5.3 and discuss the implica-
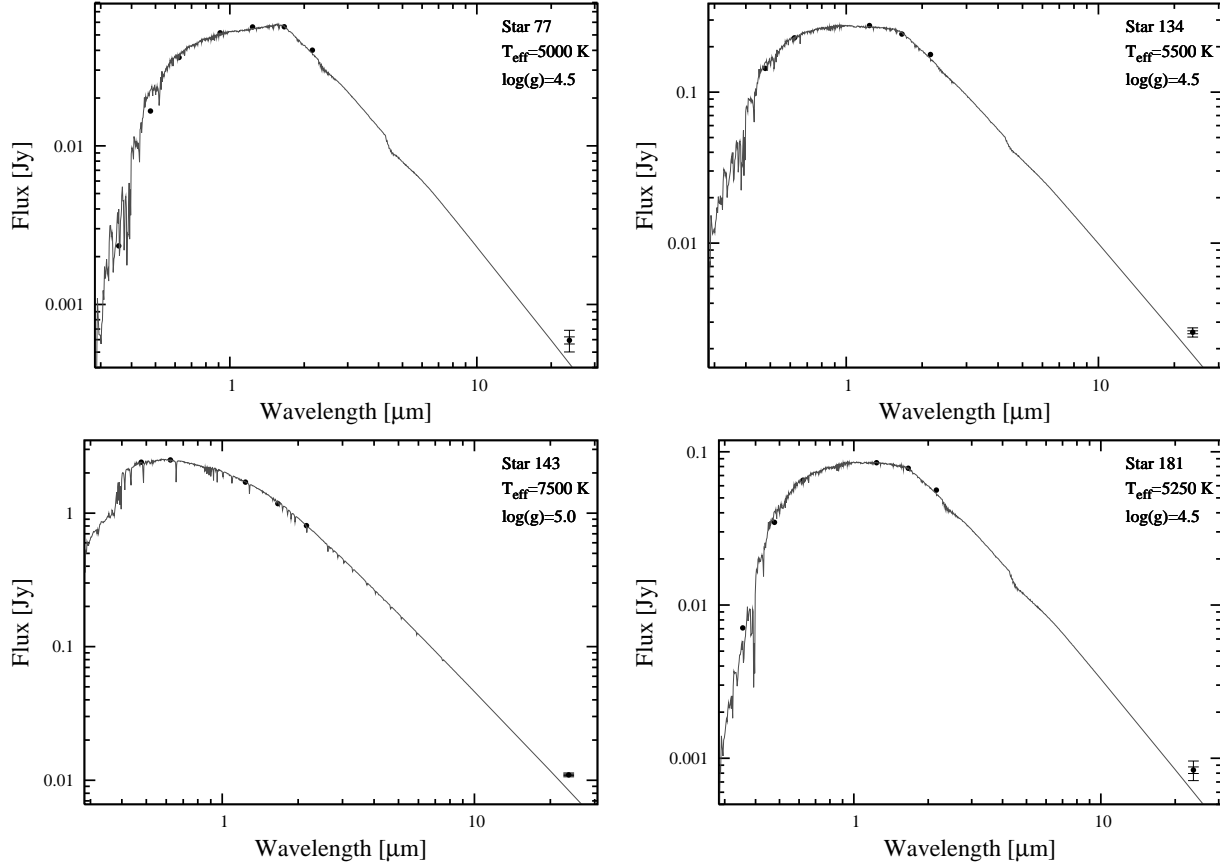
FIG. 8.— The best fitting SEDs of the debris disk candidate stars with available optical, 2MASS, and [24] photometry. The [24] photometry is plotted with 1 and 3σ errors.

tions for debris disk decay time scales in §5.4. In §5.5, we compare these results with a simple model for the incidence of episodes like the LHB around other stars.

5.1. Calulating errors on debris disk fractions

Due to the small number of observations, we estimated our debris disk fractions and associated uncertainties using a Bayesian approach, which we outline in this section.

If the fraction of objects with disks is $f_{\rm disk}$, derived from our observed number of disks (n) from a sample size of N, then the posterior probability that $f_{\rm disk}$ has a certain value will be

$$P(f_{\rm disk}|n,N) \propto P(f_{\rm disk})P(n|f_{\rm disk},N). \quad (4)$$

Here, $P(f_{\rm disk}|n,N)$ if the probability distribution for $f_{\rm disk}$, given that n and N are known. $P(f_{\rm disk})$ is the prior distribution of $f_{\rm disk}$ and $P(n|f_{\rm disk},N)$ is the probability of observing that n of N sources have a disk, assuming a certain value of $f_{\rm disk}$. $P(f_{\rm disk}|n,N)$ will be the posterior probability distribution for $f_{\rm disk}$ and $P(n|f_{\rm disk},N)$ is the likelihood function. If no prior assumption is made on the value of $f_{\rm disk}$, then the prior will be uniform, i.e. $P(f_{\rm disk}) = 1$. This will be assumed, so that all information on $f_{\rm disk}$ originates from the data itself. The likelihood function, $P(n|f_{\rm disk},N)$, is a binomial distribution, therefore

$$P(f_{\rm disk}|n,N) \propto f_{\rm disk}{}^n (1-f_{\rm disk})^{N-n}, \quad (5)$$

where the binomial coefficient has been dropped because of its non-dependence on $f_{\rm disk}$, making it irrevelant in the posterior distribution.

This equation is equivalent to a Beta (B) distribution with parameters $\alpha = n+1$ and $\beta = N-n+1$. The expectation value (posterior mean) of the B distribution is simply

$$E(f_{\rm disk}) = \frac{\alpha}{\alpha+\beta} = \frac{n+1}{N+2}, \quad (6)$$

while its mode gives the regular ratio of n/N (if $n > 1$ and $N > 2$). The 1σ confidence region can be found by integrating the central region that contains 68.3% of the probability for the B distribution. This was done in our paper by Monte Carlo-type calculations. We simulated 10^7 random variables from a B distribution and searched for the bottom and upper limits at the 15.85% and 84.15% percentiles.

We give our results with the expectation values and the upper and lower errors from the 1σ limits. We decided to use expectation values (posterior mean) over mode averages based on that our fractions are usually low making the distributions skewed. In such cases, they are better described by their mean. For example, this will give an expected debris disk fraction of

$$E(f_{\rm disk}) = \frac{1+1}{106+2} = 1.85\% \quad (7)$$

for our solar-type stars.

5.2. The decay of the debris disk fraction in early-type stars

A-type stars are well suited to search for excess emission originating from debris disks. The extended surveys

TABLE 3
THE FIELD STAR SAMPLE EXCESS RATIOS AT 24 μM AT CERTAIN AGE BINS FOR EARLY TYPE STARS (RIEKE ET AL. 2005; SU ET AL. 2006).

Age [Myr]	Excess fraction [#]	[%]
3.16 - 10	6/10	58.3 ± 14.2
10 - 31.6.........................	3/4	$66.7^{+18.7}_{-19.1}$
31.6 - 100	4/10	41.7 ± 14.2
100 - 316	13/39	34.2 ± 7.4
316 - 1000	3/31	12.1 ± 5.5

of Rieke et al. (2005) and Su et al. (2006), probed the excess fraction for A-type stars in the field and in associations between the ages of 5 and 850 Myr. Numerous observations have also determined the excess fraction for early-type stars in open clusters and associations (e.g. Young et al. 2004; Gorlova et al. 2004, 2006; Siegler et al. 2007; Cieza et al. 2008).

We compared our early spectral type excess fraction to the ones in the literature. We combined the data of Rieke et al. (2005) and Su et al. (2006), removing cluster and association members. Sources that were listed in both catalogs were adopted from Su et al. (2006), due to the improved reduction methods and photospheric model fits in the latter paper. Sources were counted as excess sources if their relative excess exceeded 15%. IRAS and ISO sources from the Rieke et al. (2005) sample were removed, due to their higher – 25% – excess thresholds. Our final age bins from the combined catalogs are listed in Table 3.

We also compared our results to those from open cluster (and OB association) surveys by other groups. We list these clusters, their excess fraction, age and the references for these parameters in Table 4. The majority of these clusters are from MIPS group papers, that used the same 15% excess level threshold as we did in our study of Praesepe. The few others used similar thresholds, or as in the case of the β Pic MG study (Rebull et al. 2008), all excess sources that were identified exceeded their 20% threshold with no sources between 15 and 20%. We plot the excess fractions from all surveys with the field star samples in the *top left* panel of Figure 9.

The fifteen open clusters and associations follow the same trend as the field star sample, with the exception of IC 2602 (Su et al. 2006) and IC 2391 (Siegler et al. 2007). Possible explanations for this deviation are explored in Siegler et al. (2007) and they conclude that the most likely cause is the lack of a statistically large sample. The peak near ~ 12 Myr observed by Currie et al. (2008) is suggested. Thereafter, the excess fraction shows a steady decline to the age of Praesepe (~ 750 Myr). Although the single A7 debris disk star we observed is not a statistically high number, the sample of 29 stars it was drawn from is high enough to indicate a real lack of debris disks around early-type stars at ~ 750 Myr.

5.3. *The decay of the debris disk fraction for solar-type stars*

Detailed studies of the frequency of debris disks as a function of system age are useful tools to characterize belts of planetesimals and their collisions around solar-type stars. They provide important proxies for

TABLE 4
THE EXCESS FRACTION AT 24 μM FOR EARLY TYPE STARS IN CLUSTERS/ASSOCIATIONS.

Name	Age [Myr]	Excess fraction [#]	[%]	Exc. Reference	Age
Upper Sco..	5±1	0/3	36.9*	1,2	11
Orion OB1b	5±1	6/22	29.2±9.2	3	12
Orion OB1a	8.5±1.5	8/21	39.1±10.2	3	12
β Pic MG ..	12^{+8}_{-4}	3/5	$57.1^{+18.6}_{-18.7}$	4	13
Upper Cen .	25±5	7/17	42.1±11.3	1,2	14
NGC 2547..	30±5	8/18	45.0±11.1	5,6	5,6
IC 2602	30±5	1/8	$20.0^{+12.3}_{-12.0}$	1	15
IC 2391	50±5	1/10	$16.7^{+10.4}_{-10.1}$	7	16
α Per	65±15	2/5	$42.9^{+18.7}_{-18.6}$	1,2	17,18
Pleiades....	115±10	2/7	$33.3^{+15.6}_{-15.5}$	1	18,19,20
Pleiades....	115±10	5/20	$27.3^{+9.5}_{-9.4}$	6	18,19,20
NGC 2516..	145±5	13/51	26.4±6.0	2	19,21
Ursa M.....	400±100	1/7	$22.2^{+13.5}_{-13.2}$	1	22,23,24
Coma Ber ..	500±50	0/5	26.4*	1,2	25
Hyades.....	625±50	1/12	$14.3^{+9.0}_{-8.8}$	1	26
Hyades.....	625±50	2/11	$23.1^{+11.5}_{-11.4}$	9	26
Praesepe ...	757±114	1/29	6.5±4.1	10	10
Praesepe ...	757±114	0/5	26.4*	1	10

REFERENCES. — (1) Su et al. (2006); (2) Rieke et al. (2005); (3) Hernández et al. (2006); (4) Rebull et al. (2008); (5) Young et al. (2004); (6) Gorlova et al. (2007); (7) Siegler et al. (2007); (8) Gorlova et al. (2006); (9) Cieza et al. (2008); (10) This work; (11) Preibisch et al. (2002); (12) Briceño et al. (2005); (13) Ortega et al. (2002); (14) Fuchs et al. (2006); (15) Stauffer et al. (1997); (16) Barrado y Navascués et al. (2004); (17) Song et al. (2001); (18) Martín et al. (2001); (19) Meynet et al. (1993); (20) Stauffer et al. (1998); (21) Jeffries et al. (2001); (22) Soderblom & Mayor (1993); (23) Castellani et al. (2002); (24) King et al. (2003); (25) Odenkirchen et al. (1998); (26) Perryman et al. (1998)
* Upper limit

TABLE 5
THE FIELD STAR SAMPLE EXCESS RATIOS AT 24 μM FOR SOLAR-TYPE STARS AT CERTAIN AGE BINS FROM THE COMPILED SAMPLE OF TRILLING ET AL. (2008), BEICHMAN ET AL. (2006) AND THE FEPS COLLABORATION (CARPENTER ET AL. 2008A,B; MEYER ET AL. 2008).

Age		Excess fraction [#]	[%]
3.16 - 10	Myr	2/12	$21.4^{+10.8}_{-10.6}$
10 - 31.6	Myr	2/8	$30.0^{+14.4}_{-14.2}$
31.6 - 100	Myr	2/38	7.5 ± 4.0
100 - 316	Myr	7/48	16.0 ± 5.1
316 - 1000	Myr	7/58	13.3 ± 4.3
1 - 3.16	Gyr	2/94	3.1 ± 1.7
3.16 - 10	Gyr	6/167	4.1 ± 1.5

comparisons between the Solar System and exoplanetary systems in terms of planetary system formation and evolution. For example, observations at 70 μm show that Kuiper-belt-like planetesimal systems around solar-type stars can be rather common ($\sim 16\%$; Trilling et al. 2008)($\sim 14\%$; Hillenbrand et al. 2008), but are not necessarily accompanied by 24 μm excess, which would be indicative of terrestrial planet formation.

To provide a large sample, we merged the 24 μm data of Trilling et al. (2008), Beichman et al. (2006) and that of the FEPS group (Carpenter et al. 2008a,b; Meyer et al. 2008) resulting in a database of 425 solar-type field stars with age estimates in the range from 3.16 Myr to 10
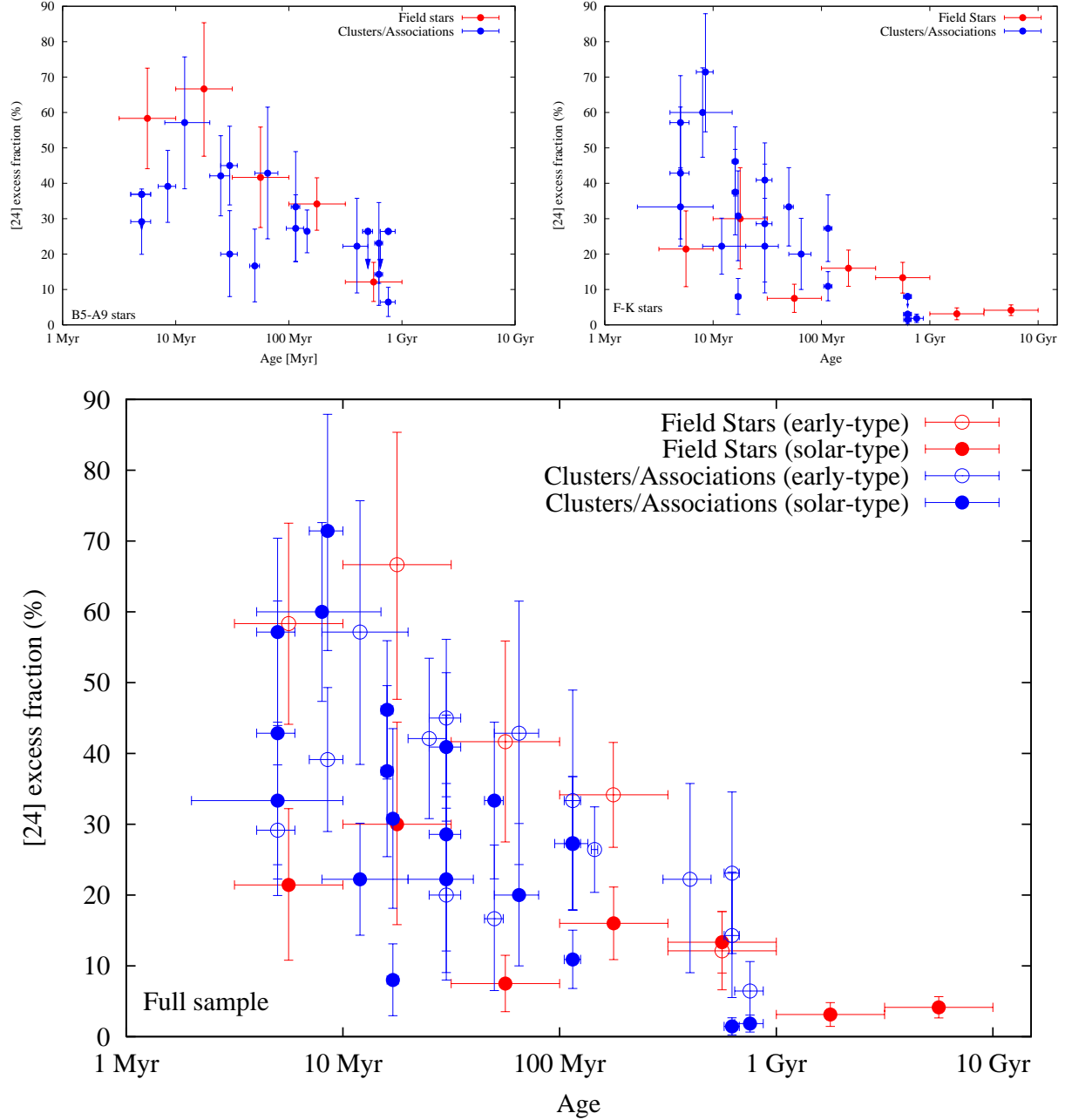
FIG. 9.— *Top Left Panel:* The decay of the debris disk fraction for early type stars. *Top Right Panel:* The decay of the debris disk fraction for solar-type stars. *Bottom Panel:* The combined plot of all excess fractions. The errors in excess fraction are the 1σ errors from the beta distribution calculations (§5.1) while the age errors are from the literature. The age "errors" for the field star sample show the age bins.

Gyr. The tables in Trilling et al. (2008) include the results of Bryden et al. (2006) and Beichman et al. (2005) with their photometry data reevaluated with the same procedures as the newer Trilling et al. (2008) sample. We divided this database into the same logarithmic age bins as we did for the early-type field star sample and calculated the debris disk fraction in these bins using the 15% threshold in excess emission at 24 μm. The debris disk fractions are summarized in Table 5.

We also compiled results at 24 μm from the literature on debris disk fractions around solar-type stars in open clusters and associations. They are summarized in Table 6. The excess fractions for the combined sample of solar-

type stars are plotted in the *top right* panel of Figure 9. The plots show a significantly larger scatter in the excess fractions for solar-type than for early-type stars. A second interesting feature is a possible environmental effect on the fraction of debris disks around solar-type stars. Although not pronounced – and possibly strongly effected by sampling biases – there seems to be higher fraction of debris disk stars in clusters/associations than in the field.

In Praesepe, the few debris disk candidate stars (from a statistically large sample of 106 stars) implies that the planetary systems in the 1-40 AU zones around solar-type stars have generally reached a quiescent phase. This

TABLE 6
THE EXCESS FRACTION IN [24] FOR SOLAR-TYPE STARS IN
CLUSTERS/ASSOCIATIONS.

Name	Age [Myr]	Excess fraction [#]	Excess fraction [%]	Exc. Reference	Age Reference
Orion OB1b	5 ± 1	7/12	57.1 ± 13.2	1	11
Upper Sco ..	5 ± 1	5/16	$33.3^{+11.1}_{-11.0}$	2	12
Upper Sco ..	5 ± 1	2/5	$42.9^{+18.7}_{-18.6}$	3	12
η Cha.......	8^{+7}_{-4}	8/13	60 ± 12.6	4	13,14
Orion OB1a	9 ± 2	4/5	$71.4^{+16.4}_{-16.9}$	1	11
β Pic MG...	12^{+8}_{-4}	5/25	22.2 ± 7.9	5	15
Lower Cen C	16 ± 1	11/24	46.2 ± 9.8	3	16
Lower Cen C	16 ± 1	5/14	$37.5^{+12.1}_{-12.0}$	2	16
Upper Cen L	17 ± 1	3/11	$30.8^{+12.7}_{-12.6}$	3	12
Upper Cen L	17 ± 1	1/23	$8.0^{+5.1}_{-5.0}$	2	12
NGC 2547 ..	30 ± 5	8/20	40.9 ± 10.5	6	6
Tuc-Hor	30 ± 5	1/7	$22.2^{+13.5}_{-13.2}$	5	17
IC 2602.....	30 ± 5	1/5	$28.6^{+16.9}_{-16.4}$	2	18
IC 2391.....	50 ± 5	5/16	$33.3^{+11.1}_{-11.0}$	7	19
α Per	65 ± 15	2/13	$20.0^{+10.1}_{-10.0}$	2	20,21
Pleiades	115 ± 10	5/53	10.9 ± 4.1	8	21,22,23
Pleiades	115 ± 10	5/20	27.3 ± 9.4	2	21,22,23
Hyades	625 ± 50	0/67	2.7^*	9	24
Hyades	625 ± 50	0/22	7.7^*	2	24
Praesepe....	757 ± 114	1/106	1.9 ± 1.2	10	10

REFERENCES. — (1) Hernández et al. (2006); (2) Carpenter et al. (2008b); (3) Chen et al. (2005); (4) Gautier et al. (2008); (5) Rebull et al. (2008); (6) Gorlova et al. (2007); (7) Siegler et al. (2007); (8) Gorlova et al. (2006); (9) Cieza et al. (2008); (10) This work; (11) Briceño et al. (2005); (12) Preibisch et al. (2002); (13) Mamajek et al. (1999); (14) Lyo et al. (2004); (15) Ortega et al. (2002); (16) Mamajek et al. (2002); (17) Rebull et al. (2008), with arbitrary errors adopted from similar age clusters; (18) Stauffer et al. (1997); (19) Barrado y Navascués et al. (2004); (20) Song et al. (2001); (21) Martín et al. (2001); (22) Meynet et al. (1993); (23) Stauffer et al. (1998); (24) Perryman et al. (1998)
* Upper limit

behavior can be compared with that of the field star sample, which levels off at a few percent at ages > 1 Gyr. This result may seem surprising given the LHB period of the Solar System, but it is actually consistent with the models of Gomes et al. (2005) and Thommes et al. (2008). The LHB was modeled in these papers to be a result of instability in the planetary system, caused by either strong interaction at the mean motion resonances of Jupiter and Saturn or that of Uranus and Neptune. In both cases the outer planetary disk is destabilized, causing planetesimals to migrate inward and initiate a collisional cascade. The models of Gomes et al. (2005) show a wide range of ages (192 Myr – 1.1 Gyr) when the LHB can occur, but they are more likely to be initiated at the earlier ages. The timing of the cascade depends on a few initial conditions that can be set to realistic parameters to give any of the solutions. The paper by Strom et al. (2005) also agrees that the LHB was a catastrophic event, lasting between 10 and 150 Myr, however they argue that the characteristics of the craters found on the inner planets originating from that epoch are more likely to be from main belt asteroids.[8]

[8] Hartmann et al. (2000) and Morbidelli et al. (2001) argued that the LHB was the tail end of a monotonically decreasing impactor population. This theory was questioned by Bottke et al. (2007), who computed the probability of the cratering records being created by it, and could rule it out at a 99.7% (3σ) confidence

The collisional cascade or "terminal cataclysm" model is also supported by recent studies of Hadean-era zircons on Earth (Trail et al. 2007).

5.4. Evolutionary differences between the debris disks around early- and solar-type stars

To illustrate the differences between the evolution of debris disks around early- and solar-type stars, we combined the top panel plots in Figure 9 in the bottom panel of the same figure. There appears to be an upper envelope to the excess fraction as a function of age, as if there were a theoretical maximum number of debris disks possible at any age. There is substantial scatter below this envelope.

Figure 9 shows that there is a subtle difference between the evolution of debris disks around early- and solar-type stars. To reduce the effects of observational biases (such as detection thresholds) and sampling differences (number of stars in clusters), we rebinned all the data to a more homogeneous sampling. We used the same logarithmic age bins as we did for the field star samples: 3.16-10, 10-31.6, 31.6-100, 100-316 Myr, and 0.316-1, 1-3.16, and 3.16-10 Gyr. The result is shown in Figure 10, along with a second plot that shows the decay trends for A, F and G spectral-type stars separately. The data for all rebinned decay trends are summarized in Table 7. The "rise-and-fall" characteristics for early-type stars is confirmed (Currie et al. 2008), but with a quick drop-off at later ages. The solar-type stars show a monotonic decaying trend that reaches a constant of a few percent at later ages. The most important feature though is that the trends have different timescales.

The fraction of infrared excesses at a given age range is set by the interplay of the occurrence rate of the collisional cascades for each system, the longevity of the dust produced in these cascades, and our ability to detect the debris at the distance of the given cluster. Detailed modeling of these processes is required to interpret the different rate of decline in the debris disk fraction between early- and solar-type stars. Although such modeling is beyond the scope of this paper, three possible explanations can be invoked to explain qualitatively the faster decline of excess fraction around solar-type stars. First, the dust must be in the 24 μm emitting regions and solar-type stars have about $50\times$ smaller disk surface area in which a collisional cascade can produce warm enough dust. Second, the orbital velocity of planetesimals in the 24 μm emitting zone will be higher around solar-type than the early-type stars, possibly accelerating the evolution of their debris disks. Third, the dust size distributions and lifetimes are different for the two groups of stars. These issues will be discussed in a forthcoming paper (Gáspár et al. 2009).

5.5. Our results in context with the Late Heavy Bombardment

The cratering record of all non geologically active rocky planets and moons in the inner Solar System reveal a period of very intense past bombardment. Geochronology of the lunar cratering record shows that this bombardment ended abruptly at $\sim$ 700 Myr (see e.g. Tera et al. 1973, 1974; Chapman et al. 2007), but the scarcity of

level.
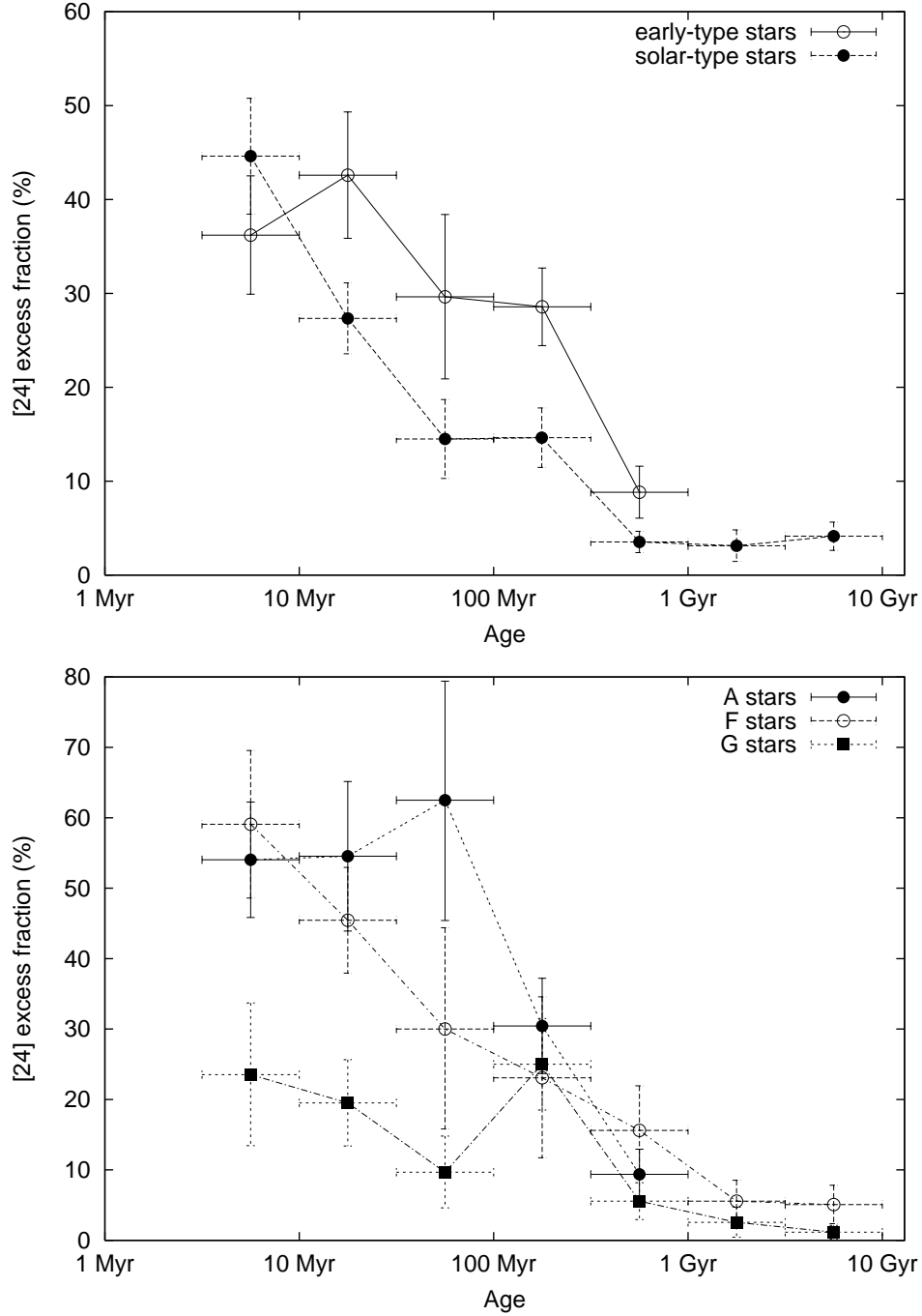
FIG. 10.— *Top panel:* The difference between the decaying trend for early- and solar-type stars, in a binned data plot. *Bottom panel:* The difference between the decaying trend for A, F and G spectral-type stars, in a binned data plot. The errors in the excess fraction are from beta distribution calculations (§5.1), while the "error bars" in the ages show the age bins. The numerical values for the data points are summarized in Table 7.

the lunar rock record prior to this event hinders accurate assessment of the temporal evolution of the impact rates or the length of the bombardment period. Dynamical simulations of different possible impactor populations show that an unrealistically massive impactor population would be required to maintain the impact rate measured at the end of the bombardment for a prolonged period, thus convincingly arguing for the bombardment being a short-duration spike in the impact rate (Bottke et al. 2007). A possible explanation for this is that a dynamical instability initiated by the migration of the giant plan-

ets caused minor planetary bodies to migrate inwards from the outer region of the Solar System, bombarding the inner planets. Modeling shows that this scenario can occur over a wide range of ages (Gomes et al. 2005). Strom et al. (2005) show that it is possible instead that main belt asteroids bombarded the planetary system.

We performed a Monte Carlo simulation to evaluate our observed debris disk fraction in the context of the evidence from the LHB. Our goal was to constrain the fraction of the solar-type stars that undergo LHB (or fine dust generation) and the duration of these events.

TABLE 7
The percent of debris disks in a rebinned distribution, as a function of stellar spectral-type.

Age		Early-type stars Excess fraction		Solar-type stars Excess fraction		A-type stars Excess fraction		F-type stars Excess fraction		G-type stars Excess fraction	
		[#]	[%]	[#]	[%]	[#]	[%]	[#]	[%]	[#]	[%]
3.16 - 10	Myr	20/56	36.2±6.3	28/63	44.6±6.2	19/35	54.05±8.2	12/20	59.09±10.5	3/15	$23.5^{+10.1}_{-10.2}$
10 - 31.6	Myr	22/52	42.6±6.7	37/137	27.3±3.8	11/20	54.55±10.6	19/42	45.45±7.5	7/39	19.5±6.1
31.6 - 100	Myr	7/25	$29.6^{+8.8}_{-8.7}$	9/67	14.5±4.2	4/6	$62.50^{+17.1}_{-16.9}$	2/8	$30.00^{+14.2}_{-14.4}$	2/29	9.7±5.1
100 - 316	Myr	33/117	28.6±4.1	17/121	14.6±3.2	13/44	30.43±6.8	2/11	$23.08^{+11.4}_{-11.5}$	10/42	25.0±6.5
316 - 1000	Myr	8/100	8.8±2.8	8/253	3.5±1.1	5/62	9.38±3.6	4/30	15.62±6.3	3/70	5.6±2.6
1 - 3.16	Gyr	-	-	2/94	3.1±1.7	-	-	2/52	5.56±3.0	0/37	$2.6^{+2.1}_{-2.2}$
3.16 - 10	Gyr	-	-	6/167	4.1±1.5	-	-	2/57	5.08±2.7	0/85	1.2±1.0

Fig. 11.— The probability of detecting the 1-3% (2/(106+29)) debris disk fraction observed at Praesepe, as a function of the percentage of 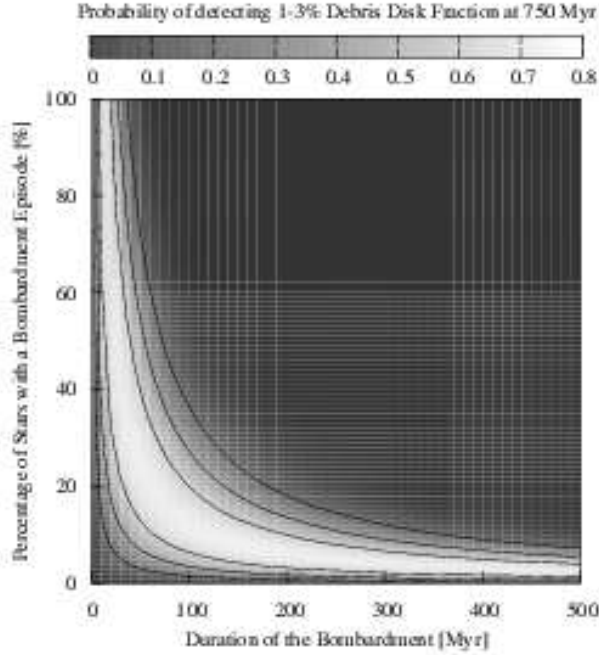stars that undergo LHB type debris disk generation and the duration of the events. The contour lines are at 20, 40 and 60% probability.

We presumed in our models that all LHB events could be detected in the existing debris disk surveys and that they had an equal probability of occurring once from 100 Myr to 1 Gyr. Both of these are strong assumptions. There is significant uncertainty on how much dust was generated and under what time scales during the LHB, making it difficult to relate the LHB unambiguously to debris disks. However, given that *Spitzer* measurements of 24 μm excess emission are typically sensitive to a collisional cascade involving mass on the order of a few lunar masses, and that such an episode has clearing time scale $\gtrsim 2$ Myr (Grogan et al. 2001), it seems plausible that the destruction of a few large asteroids can be detected in most observed systems. In our code we modeled clusters with 135 (106+29) members in 20000 simulations. We varied the overall percentage of stars that will ever generate a debris disk from 0 to 100 % and the duration of their bombardment episodes from 0 to 500 Myr. If the number of disks at 750 Myr were within our measured excess fraction of 1-3%, the simulation was tagged as be-

ing consistent with our measurements, else it was tagged inconsistent. The overall probability of a given parameter pair is given by dividing the number of consistent simulations at a certain total disk fraction and duration timescale by the number of simulations (20000).

Our calculated probability map is shown in Figure 11. The plot shows that the results are degenerate in the parameter space of dt and $p_{\rm d}$, with dt being the duration of a bombardment episode and $p_{\rm d}$ the percentage of stars to ever undergo such an event. Between the extremes of a very large percentage of the stars undergoing debris disk generation, but with a very short lifetime ($\sim$ 5-10 Myr) and a very small percentage (< 5 %), with a long (> 300 Myr) lifetime there is a continuous set of solutions.

Our simple model allows the quantitative assessment of the probability of different types of LHB-like episodes. For example, we can exclude at a 3 % significance level that 60% of the stars undergo major orbital rearrangements, if this leads to debris production over 100 Myr. Similarly, very short debris producing events are unlikely, because they would not produce observable disks, inconsistent with our results.

If we seek to evaluate the probability of strictly LHB-like debris producing episodes we can fix the length of the episode to 75 Myr, consistent with the duration estimated for the inner Solar System and the other timescales discussed in §5.3. In this case our results show that up to 15-30 % of the stars should undergo such a major orbital reorientation during the first Gyr of their evolution to be consistent with our modeling.

6. SUMMARY

We conducted a 24 μm photometric survey for debris disks in the nearby ($\sim$ 180 pc) relatively old (750 Myr) Praesepe open cluster. The combined sample of SDSS, Webda, and 2MASS gave us a robust highly probable cluster member list. With simultaneous fitting of cluster distance and age we derived a series of solutions for both parameters as a function of metallicity (see Appendix). Our derived age for Praesepe is 757 Myr ($\pm$ 114 Myr at 3σ confidence) and a distance of 179 pc ($\pm$ 6 pc at 3σ confidence), not allowing for systematic errors.

Out of the 193 cluster members that we detected at all wavelengths in the combined catalog, 29 were early (B5-A9) and 164 later (F0-M0) spectral types. We found one star in the early and three in the later spectral type groups that show excess emission. Up to near our completeness limit, with one debris disk star, there are 106 sources in the later spectral-type sample. This result shows that only $6.5 \pm 4.1\%$ of early- and $1.9 \pm 1.2\%$ of

solar-type stars are likely to possess debris disks in the 1-40 AU zones. These values are similar to that found for old (> 1 Gyr) field stars.

We place our results in context with the Late Heavy Bombardment theory of the Solar System. With simple Monte Carlo modeling we show that our observations are consistent with 15-30% of the stars undergoing a major re-arrangement of the planetary orbits and a subsequent LHB-like episode once in their lifetime, with a duration period of 50-100 Myr.

We also summarize the results in the literature on the decay timescales of debris disks around early- and solar-type stars. We find that the decay timescale for solar-type stars is shorter than for earlier-type stars.

APPENDIX

AGE AND DISTANCE ESTIMATE

The precise value of the cluster age is important in constraining the debris disk fraction as a function of stellar age. The age and distance of Praesepe have been a matter of debate, especially since it is an important step in the galactic distance ladder. The estimated ages spread from $\log t = 8.6$ all the way to $\log t = 9.15$ (400 Myr – 1.42 Gyr)[9]. Most papers list it as a coeval cluster with the Hyades because of their similar metallicities and spatial motions (see, e.g., Barrado y Navascués et al. 1998). The Hyades on the other hand has a better defined age of $\log t \approx 8.8$ (625±50 Myr)(Perryman et al. 1998; Lebreton et al. 2001). If the clusters are coeval, their ages should agree within close limits.

Aside from using pulsating variables (Tsvetkov 1993) or stellar rotation (Pace & Pasquini 2004) to estimate the age of the cluster, the only method is to fit theoretical stellar evolution turnoff points on the observed CMD. This procedure involves a precise simultaneous fitting of the cluster distance, reddening, metallicity and age.

The metallicity of Praesepe has been revisited many times. The value of Boesgaard & Budge (1988) of [Fe/H] = 0.13 ± 0.07 is usually accepted. An et al. (2007), with new spectroscopic measurements, obtained a value of [Fe/H] = 0.11 ± 0.03, also showing that the cluster is slightly metal rich. This fact has been overlooked in some studies that have used solar values for metallicity, and which therefore underestimate the cluster distance and overestimate its age.
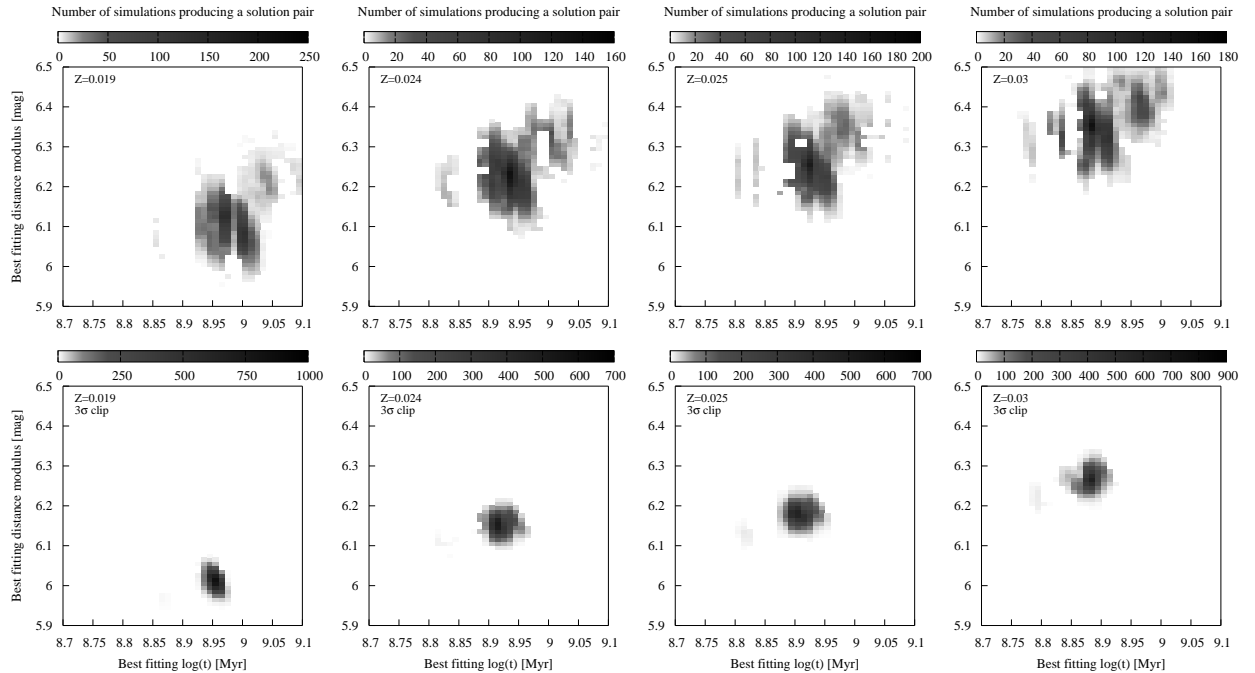
FIG. 12.— The 2D probability maps show the number of solutions that were given for certain solution pairs by the Monte Carlo isochrone fitting algorithm. The top row shows the fitting for the full sample, while the bottom row gives the solutions after a 3σ clipping iterational step. The fitted metallicities are $Z = 0.019, 0.024, 0.025$ and 0.03.

[9] Allen (1973); Vandenberg & Bridges (1984); Tsvetkov (1993); González-García et al. (2006)
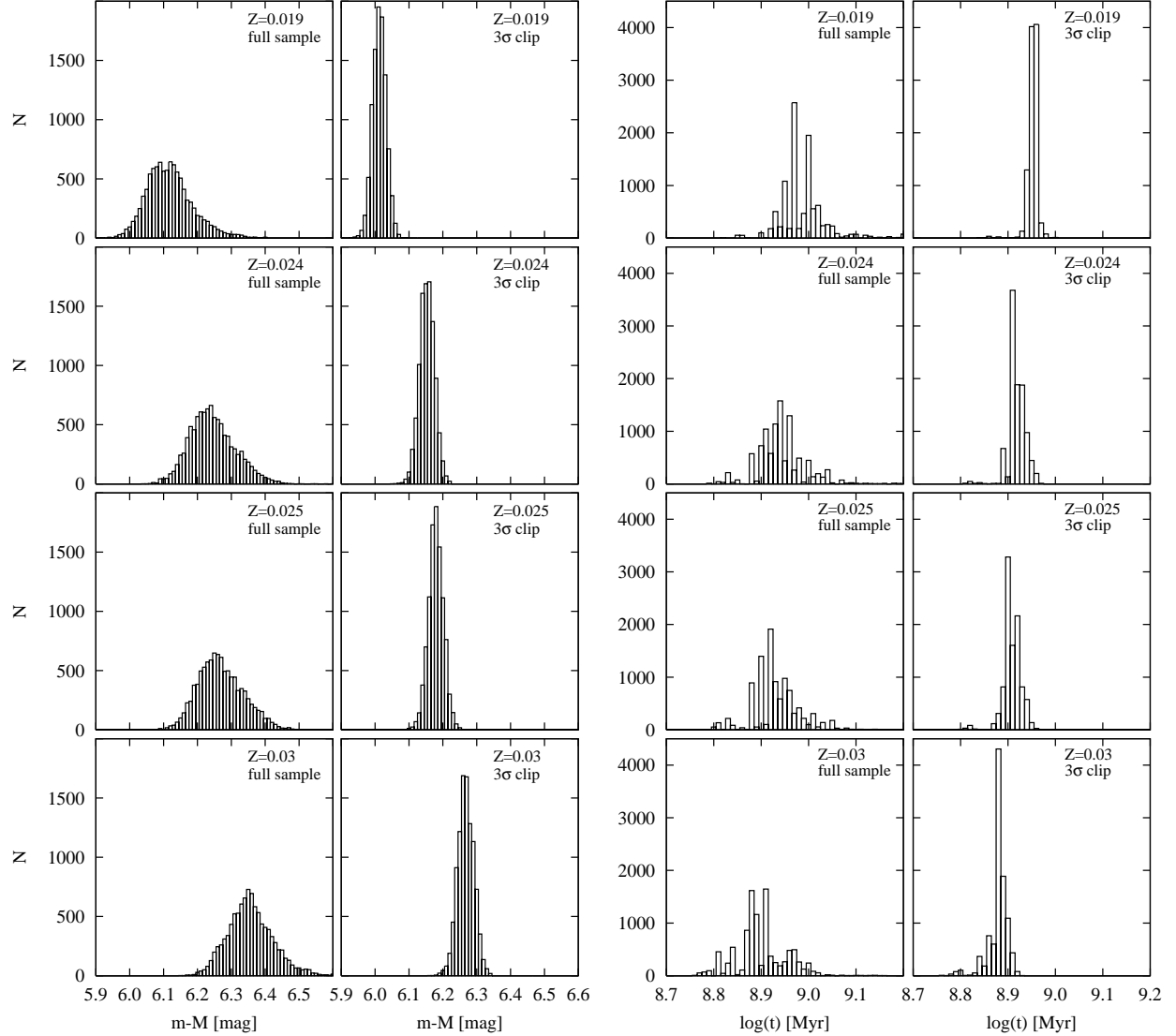
FIG. 13.— These plots show the 1D representation of Figure 12, separately for $m - M$ and $\log(t)$. The distributions get much narrower after the 3σ clipping iterations. These plots clearly show that as you go to more metal rich isochrones, the best fitting isochrones will be younger and more distant.

The distance to Praesepe has been determined with many methods, yielding slight differences among the measured values. Gatewood & de Jonge (1994) used the Multichannel Astrometric Photometer (MAP) of the Thaw Refractor of the University of Pittsburgh to determine a weighted mean parallax of $\pi = 5.21$ mas for five cluster member stars. The geometric method used by Loktin (2000) determines the apparent variation of the angular diameter of the cluster as it moves along the line of sight and estimates the distance to the cluster from it. The basic idea of this method is very similar to that of the convergent point method. The photometric distances (main-sequence fitting) seem to show a large scatter. We summarize the previous distance measurements and the methods used to obtain the values in Table 8.

We determined the distance and age of the cluster by simultaneously fitting the distance modulus and the age with isochrones. The photometry values we used were our best SDSS g and r band data, with the corrections explained in §3. We did not include reddening in our color values, because it can be neglected towards Praesepe (E(B-V)=0.027 ± 0.004 mag; Taylor (2006)). Since the plotted CMD of Praesepe clearly showed a vertical trend at the later spectral type stars at $g - r \approx 1.2$, we only fitted cluster member points with $g - r < 1.2$ (fitting the distance modulus to a vertical trend is impossible and only adds errors to the fit). The isochrones for the fit were obtained from the Padova group website[10], where isochrones of any age and metallicity can be generated for a large number of photometric systems, such as the SDSS system (Girardi et al. 2004). These isochrones are similar to the empirical isochrones produced by An et al. (2007).

Since the metallicity of the cluster is still debated, we fitted isochrone sets for all metallicities in the literature. Assuming that metallicities are solar scaled, we set [Fe/H]=[M/H]. We fitted the following: [Fe/H]=0.13 (Z=0.025;

[10] http://pleiadi.pd.astro.it/
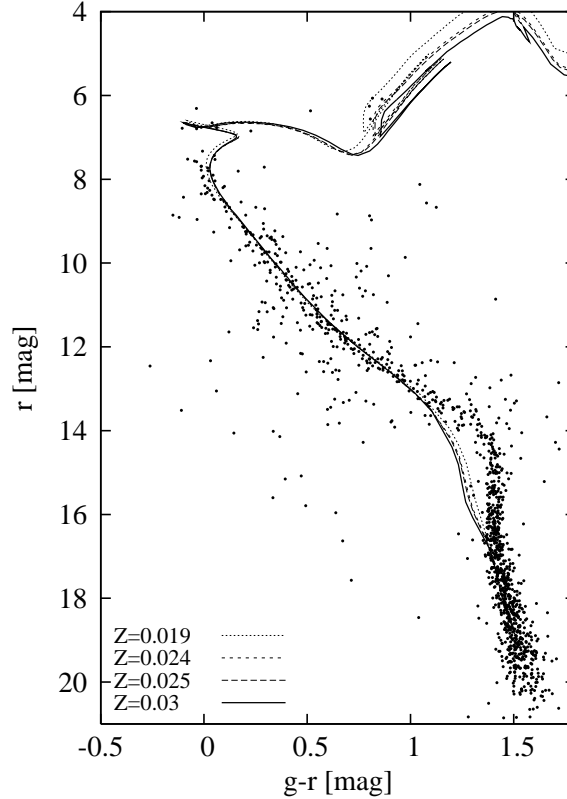
FIG. 14.— The best fitting isochrones for all metallicities in the literature plus solar. The dotted line isochrone that deviates from the rest at high luminosities is the solar (Z=0.019) isochrone.

Boesgaard & Budge 1988), [Fe/H]=0.11 (Z=0.024; An et al. 2007) and [M/H]=0.2 (Z=0.03; An et al. 2007). The two values from the An et al. (2007) paper are from [Fe/H], determined from spectroscopy, and an [M/H] value from isochrone fitting. We also fitted solar metallicity isochrones to show the errors they give in the age and distance determinations.

We calculated the best fit via Monte Carlo (i.e. bootstrap) method. We generated 10,000 new samples with the same number of sources as in the original cluster member list. As with the bootstrap method, the members in the new samples were randomly picked from the original, resulting in multiple picks of a few sources and null of others. The best fitting isochrones (as a function of age and distance) to these mock samples were found by χ^2 minimization. We computed χ^2 from each fit as

$$\chi^2 = \sum (\Delta r^2 + \Delta (g-r)^2), \tag{A1}$$

where Δr^2 is the r magnitude difference while $\Delta (g-r)^2$ is the color difference from the closest point of the isochrone model. By finding the closest point of the isochrones we not only fit the luminosity difference, but an actual distance from the isochrone, thus allowing points to be horizontally offset. We did not weight our fit by photometric errors, because the brightest members (that are most crucial in the age determination) did not have quoted errors, while the errors of the SDSS data cannot be trusted brighter than 14th magnitude. The means and errors in age and distance modulus of the best fitting isochrone (for all metalicities) were calculated from the distribution of solutions given by the bootstrap method. Following an initial fit, we removed stars that were further than $3\sigma_{m-M}$ magnitude from the best fitting isochrones and reran the Monte Carlo code. The best fit value is given as the arithmetic mean and its error as its standard deviation.

The 2D errors for the fits are shown in Figure 12, both for the full and for the clipped samples. The histograms of the distance modulus and age fits are shown in Figure 13, both for the full and for the clipped samples also. The results of the fitting for the $3\sigma_{m-M}$ clipped sample are summarized in Table 9 quoting the 1σ errors. These errors are purely from the fitting procedure, and do not include possible systematic errors such as those from isochrone models, reddening, extinction and photometry.

The best fitting isochrones for the four metallicities are shown in Figure 14. All isochrones seem to deviate from the observed trend at $g-r > 1.2$ magnitude. This is either due to errors in the calculated isochrones or to the membership criteria of Kraus & Hillenbrand (2007), who used estimated T_{eff} and luminosity values from photometry fitted SEDs and theoretical Hertzsprung-Russell diagrams.

We adopted the metallicity of Z=0.03 (An et al. 2007) to give a final estimate of the cluster's age and distance. We chose this metallicity to ensure comparability, since An et al. (2007) deduced it from isochrone fitting also. The distance modulus of our best fit for this metallicity is $m - M = 6.267 \pm 0.024$ at 1σ confidence, within errorbars of the

TABLE 8
THE DISTANCE-MODULUS OF PRAESEPE IN THE LITERATURE.

Reference	Method used	$m - M$ [mag]
Nissen (1988)	Photometric	6.05
Mermilliod et al. (1990)	Photometric	6.2
Hauck (1981)	Photometric[a]	6.26±0.23
Vandenberg & Bridges (1984)	Photometric	5.85
An et al. (2007)	Photometric[b]	6.33 ± 0.04
Gatewood & de Jonge (1994)	Parallax	6.42 ± 0.33
Loktin (2000)	Geometric	6.16 ± 0.19
This paper	Photometric	6.267 ± 0.024

[a] Using Lutz-Kelker corrections (Lutz & Kelker 1973).
[b] Using empirically corrected isochrones.

TABLE 9
THE SOLUTIONS FOR THE FITTING OF ISOCHRONES VIA TWO PARAMETERS FOR SOLAR AND THE
METALLICITIES FOUND IN THE LITERATURE GIVEN WITH 1σ ERRORS. THESE VALUES ARE THE ONES
DETERMINED AFTER THE 3σ CLIPPING ITERATION.

Metallicity	$m - M$ [mag]	Age [$\log t$]
[Fe/H] = 0.00	6.012 ± 0.020	8.952 ± 0.011
[Fe/H] = 0.13[a]	6.153 ± 0.022	8.918 ± 0.018
[Fe/H] = 0.11[b]	6.179 ± 0.022	8.908 ± 0.019
[M/H] = 0.20[b]	6.267 ± 0.024	8.879 ± 0.020

[a] Boesgaard & Budge (1988)
[b] An et al. (2007)

value of An et al. (2007) ($m - M = 6.33 \pm 0.04$ mag). The errorbars on distance are small at 3σ and comparable to the diameter of the cluster's central region (~ 6 pc). The age of the cluster is determined to be $\log t = 8.879 \pm 0.020$ (757 ± 36 Myr) at 1σ confidence. The errorbars on cluster age are significantly smaller than in papers before and help to pin down the decay trend at ages between 0.5 and 1 Gyr. The bootstrap Monte Carlo isochrone fitting method we introduce here turned out to be a very effective and successful way to determine cluster distance and age, and to estimate the errors of these parameters.

REFERENCES

Allen, C. W. 1973, London: University of London, Athlone Press, —c1973, 3rd ed.,

An, D., Terndrup, D. M., Pinsonneault, M. H., Paulson, D. B., Hanson, R. B., & Stauffer, J. R. 2007, ApJ, 655, 233

Andruk, V., Kharchenko, N., Schilbach, E., & Scholz, R. D. 1995, Astronomische Nachrichten, 316, 225

Anthony-Twarog, B. J. 1982, ApJ, 255, 245

Aumann, H. H., et al. 1984, ApJ, 278, L23

Backman, D. E., & Paresce, F. 1993, Protostars and Planets III, 1253

Backman, D., et al. 2009, ApJ, 690, 1522

Barrado y Navascués, D., Stauffer, J. R., & Randich, S. 1998, ApJ, 506, 347

Barrado y Navascués, D., Stauffer, J. R., & Jayawardhana, R. 2004, ApJ, 614, 386

Beichman, C. A., et al. 2005, ApJ, 622, 1160

Beichman, C. A., et al. 2006, ApJ, 652, 1674

Boesgaard, A. M., & Budge, K. G. 1988, ApJ, 332, 410

Bottke, W. F., Levison, H. F., Nesvorný, D., & Dones, L. 2007, Icarus, 190, 203

Bouvier, J., Duchêne, G., Mermilliod, J.-C., & Simon, T. 2001, A&A, 375, 989

Briceño, C., Calvet, N., Hernández, J., Vivas, A. K., Hartmann, L., Downes, J. J., & Berlind, P. 2005, AJ, 129, 907

Bryden, G., et al. 2006, ApJ, 636, 1098

Carpenter, J. M., et al. 2008a, arXiv:0810.1003

Carpenter, J. M., et al. 2008b, ApJS, 179, 423

Castelaz, M. W., Persinger, T., Stein, J. W., Prosser, J., & Powell, H. D. 1991, AJ, 102, 2103

Castellani, V., Degl'Innocenti, S., Prada Moroni, P. G., & Tordiglione, V. 2002, MNRAS, 334, 193

Castelli, F. & Kurucz, R.L. 2003, in Poster Papers, IAU Symp. 210: Modelling of Stellar Atmospheres, ed. N. Piskunov, W. W. Weiss & D. F. Gray (San Francisco: ASP), 20

Chapman, C. R., Cohen, B. A., & Grinspoon, D. H. 2007, Icarus, 189, 233

Chen, C. H., Jura, M., Gordon, K. D., & Blaylock, M. 2005, ApJ, 623, 493

Cieza, L. A., Cochran, W. D., & Augereau, J.-C. 2008, ApJ, 679, 720

Cox, A. N. 2000, Allen's astrophysical quantities, 4th ed. Publisher: New York: AIP Press; Springer, 2000. Editedy by Arthur N. Cox. ISBN: 0387987460

Currie, T., Kenyon, S. J., Balog, Z., Rieke, G., Bragg, A., & Bromley, B. 2008, ApJ, 672, 558

Dickens, R. J., Kraft, R. P., & Krzeminski, W. 1968, AJ, 73, 6

Dobbie, P. D., et al. 2006, MNRAS, 369, 383

Dominik, C., & Decin, G. 2003, ApJ, 598, 626

Engelbracht et al. 2007, astro-ph, 07042195, to be published in PASP

Fuchs, B., Breitschwerdt, D., de Avillez, M. A., Dettbarn, C., & Flynn, C. 2006, MNRAS, 373, 993

Fukugita, M., Ichikawa, T., Gunn, J. E., Doi, M., Shimasaku, K., & Schneider, D. P. 1996, AJ, 111, 1748

Franciosini, E., Randich, S., & Pallavicini, R. 2003, A&A, 405, 551

Gatewood, G., & de Jonge, J. K. 1994, ApJ, 428, 166

Gautier, T. N., III, et al. 2007, ApJ, 667, 527

Gautier, T. N., III, Rebull, L. M., Stapelfeldt, K. R., & Mainzer, A. 2008, ApJ, 683, 813

Girardi, L., Grebel, E. K., Odenkirchen, M., & Chiosi, C. 2004, A&A, ssss422, 205

Gomes, R., Levison, H. F., Tsiganis, K., & Morbidelli, A. 2005, Nature, 435, 466

González-García, B. M., Zapatero Osorio, M. R., Béjar, V. J. S., Bihain, G., Barrado Y Navascués, D., Caballero, J. A., & Morales-Calderón, M. 2006, A&A, 460, 799

Gordon, K.D., et al. 2005, PASP, 117, 503

Gorlova, N., et al. 2004, ApJS, 154, 448

Gorlova, N., Rieke, G. H., Muzerolle, J., Stauffer, J. R., Siegler, N., Young, E. T., & Stansberry, J. H. 2006, ApJ, 649, 1028

Gorlova, N., Balog, Z., Rieke, G. H., Muzerolle, J., Su, K. Y. L., Ivanov, V. D., & Young, E. T. 2007, ApJ, 670, 516

Grogan, K., Dermott, S. F., & Durda, D. D. 2001, Icarus, 152, 251

Habing, H. J., et al. 2001, A&A, 365, 545

Halbwachs, J. L., Mayor, M., Udry, S., & Arenou, F. 2003, A&A, 397, 159

Hambly, N. C., Steele, I. A., Hawkins, M. R. S., & Jameson, R. F. 1995, A&AS, 109, 29

Hartmann, W. K., Ryder, G., Dones, L., & Grinspoon, D. 2000, Origin of the earth and moon, edited by R.M. Canup and K. Righter and 69 collaborating authors. Tucson: University of Arizona Press., p.493-512, 493

Hauck, B. 1981, A&A, 99, 207

Hernández, J., Briceño, C., Calvet, N., Hartmann, L., Muzerolle, J., & Quintero, A. 2006, ApJ, 652, 472

Hillenbrand, L. A., et al. 2008, ApJ, 677, 630

Jeffries, R. D., Thurston, M. R., & Hambly, N. C. 2001, A&A, 375, 863

Jester, S., et al. 2005, AJ, 130, 873

Johnson, H. L. 1952, ApJ, 116, 640

Jones, B. F., & Cudworth, K. 1983, AJ, 88, 215

Jones, B. F., & Stauffer, J. R. 1991, AJ, 102, 1080

Jordi, K., Grebel, E. K., & Ammon, K. 2006, A&A, 460, 339

Kim, J. S., et al. 2005, ApJ, 632, 659

King, J. R., Villarreal, A. R., Soderblom, D. R., Gulliver, A. F., & Adelman, S. J. 2003, AJ, 125, 1980

Klein Wassink, W. J. 1927, Publications of the Kapteyn Astronomical Laboratory Groningen, 41, 1

Kraus, A. L., & Hillenbrand, L. A. 2007, AJ, 134, 2340

Lebreton, Y., Fernandes, J., & Lejeune, T. 2001, A&A, 374, 540

Loktin, A. V. 2000, Astronomy Letters, 26, 657

Lutz, T. E., & Kelker, D. H. 1973, PASP, 85, 573

Lutz, T. E., & Lutz, J. H. 1977, AJ, 82, 431

Lyo, A.-R., Lawson, W. A., Feigelson, E. D., & Crause, L. A. 2004, MNRAS, 347, 246

Mamajek, E. E., Lawson, W. A., & Feigelson, E. D. 1999, ApJ, 516, L77

Mamajek, E. E., Meyer, M. R., & Liebert, J. 2002, AJ, 124, 1670

Mamajek, E. E., Meyer, M. R., Hinz, P. M., Hoffmann, W. F., Cohen, M., & Hora, J. L. 2004, ApJ, 612, 496

Martín, E. L., Dahm, S., & Pavlenko, Y. 2001, Astrophysical Ages and Times Scales, 245, 349

Mason, B. D., Hartkopf, W. I., McAlister, H. A., & Sowell, J. R. 1993, AJ, 106, 637

Mendoza, E. E. 1967, Boletin de los Observatorios Tonantzintla y Tacubaya, 4, 149

Mermilliod, J.-C., Weis, E. W., Duquennoy, A., & Mayor, M. 1990, A&A, 235, 114

Mermilliod, J.-C., Duquennoy, A., & Mayor, M. 1994, A&A, 283, 515

Mermilliod, J.-C., & Mayor, M. 1999, A&A, 352, 479

Meyer, M. R., et al. 2004, ApJS, 154, 422

Meyer, M. R., et al. 2008, ApJ, 673, L181

Meynet, G., Mermilliod, J.-C., & Maeder, A. 1993, A&AS, 98, 477

Morbidelli, A., Petit, J.-M., Gladman, B., & Chambers, J. 2001, Meteoritics and Planetary Science, 36, 371

Nissen, P. E. 1988, A&A, 199, 146

Odenkirchen, M., Soubiran, C., & Colin, J. 1998, New Astronomy, 3, 583

Oja, T. 1985, A&AS, 61, 331

Ortega, V. G., de la Reza, R., Jilinski, E., & Bazzanella, B. 2002, ApJ, 575, L75

Pace, G., & Pasquini, L. 2004, A&A, 426, 1021

Paparó, M., & Kolláth, Z. 1990, Confrontation Between Stellar Pulsation and Evolution, 11, 336

Papovich, C., et al. 2004, ApJS, 154, 70

Perryman, M. A. C., et al. 1998, A&A, 331, 81

Preibisch, T., Brown, A. G. A., Bridges, T., Guenther, E., & Zinnecker, H. 2002, AJ, 124, 404

Randich, S., & Schmitt, J. H. M. M. 1995, A&A, 298, 115

Rebull, L. M., et al. 2008, ApJ, 681, 1484

Rieke, G. H., et al. 2004, ApJS, 154, 25

Rieke, G. H., et al. 2005, ApJ, 620, 1010

Rieke, G. H., et al. 2008, AJ, 135, 2245

Siegler, N., Muzerolle, J., Young, E. T., Rieke, G. H., Mamajek, E. E., Trilling, D. E., Gorlova, N., & Su, K. Y. L. 2007, ApJ, 654, 580

Silverstone, M. D., et al. 2006, ApJ, 639, 1138

Soderblom, D. R., & Mayor, M. 1993, AJ, 105, 226

Song, I., Caillault, J.-P., Barrado y Navascués, D., & Stauffer, J. R. 2001, ApJ, 546, 352

Spangler, C., Sargent, A. I., Silverstone, M. D., Becklin, E. E., & Zuckerman, B. 2001, ApJ, 555, 932

Stapelfeldt, K. R., et al. 2004, ApJS, 154, 458

Stauffer, J. 1982, PASP, 94, 678

Stauffer, J. R., Hartmann, L. W., Prosser, C. F., Randich, S., Balachandran, S., Patten, B. M., Simon, T., & Giampapa, M. 1997, ApJ, 479, 776

Stauffer, J. R., Schultz, G., & Kirkpatrick, J. D. 1998, ApJ, 499, L199

Stauffer, J. R., et al. 2005, AJ, 130, 1834

Strom, R. G., Malhotra, R., Ito, T., Yoshida, F., & Kring, D. A. 2005, Science, 309, 1847 01

Su, K. Y. L., et al. 2005, ApJ, 628, 487

Su, K. Y. L., et al. 2006, ApJ, 653, 675

Su, K. Y. L., Rieke, G. H., Stapelfeldt, K. R., Smith, P. S., Bryden, G., Chen, C. H., & Trilling, D. E. 2008, ApJ, 679, L125

Taylor, B. J. 2006, AJ, 132, 2453

Tera, F., Papanastassiou, D. A., & Wasserburg, G. J. 1973, Lunar and Planetary Institute Conference Abstracts, 4, 723

Tera, F., Papanastassiou, D. A., & Wasserburg, G. J. 1974, Earth and Planetary Science Letters, 22, 1

Thommes, E. W., Bryden, G., Wu, Y., & Rasio, F. A. 2008, ApJ, 675, 1538

Trail, D., Mojzsis, S. J., & Harrison, T. M. 2007, Geochim. Cosmochim. Acta, 71, 4044

Trilling, D. E., et al. 2008, ApJ, 674, 1086

Tsvetkov, T. G. 1993, Ap&SS, 203, 247

Upgren, A. R., Weis, E. W., & Deluca, E. E. 1979, AJ, 84, 1586

Vandenberg, D. A., & Bridges, T. J. 1984, ApJ, 278, 679

Wang, J. J., Chen, L., Zhao, J. H., & Jiang, P. F. 1995, A&AS, 113, 419

Weis, E. W. 1981, PASP, 93, 437

Wyatt, M. C., Smith, R., Su, K. Y. L., Rieke, G. H., Greaves, J. S., Beichman, C. A., & Bryden, G. 2007, ApJ, 663, 365

Young, E. T., et al. 2004, ApJS, 154, 428

Zhao, C., & Newberg, H. J. 2006, ArXiv Astrophysics e-prints, arXiv:astro-ph/0612034

TABLE 1
PHOTOMETRY OF PRAESEPE MEMBERS IN THE [24] BAND

#	α_{2000} [h:m:s]	δ_{2000} [°:′:″]	g* [mag]	r* [mag]	K$_{2MASS}$ [mag]	[24]† [mag]	F$_{24}$† [mJy]	μ_α [mas yr^{-1}]	μ_δ [mas yr^{-1}]	W#‡	2MASS
1	8:36:29.83	18:57:56.52	9.57	9.33*	8.30±0.01	8.23±0.05	3.54± 0.15	-34.60	-12.60	-	08362985+1857570
2	8:36:48.95	19:15:26.06	11.54*	10.92*	9.69±0.02	9.35±0.06	1.26± 0.07	-36.30	-12.80	-	08364896+1915265
3	8:37:02.04	19:36:17.42	9.34	9.06*	8.06±0.01	8.01±0.02	4.32± 0.09	-34.30	-13.00	-	08370203+1936171
4	8:37:16.35	19:29:11.58	14.67	13.38	10.47±0.02	10.06±0.07	0.65± 0.04	-34.70	-15.40	267	08371635+1929103
5	8:37:18.29	19:41:56.33	11.75	11.23	9.80±0.02	9.69±0.05	0.93± 0.04	-37.20	-15.20	268	08371829+1941564
6	8:37:26.51	19:29:13.06	14.48	13.33	10.83±0.02	10.77±0.15	0.34± 0.05	-42.70	-14.40	274	08372638+1929128
7	8:37:27.58	19:37:03.29	11.97	11.40	9.81±0.02	9.75±0.06	0.87± 0.04	-34.10	-12.60	277	08372755+1937033
8	8:37:27.95	19:33:45.25	9.91*	9.64	8.46±0.02	8.48±0.02	2.80± 0.06	-36.60	-13.20	2	08372793+1933451
9	8:37:28.22	19:09:44.32	9.65	9.37*	8.40±0.01	8.39±0.02	3.06± 0.05	-36.20	-13.40	3	08372819+1909443
10	8:37:33.84	20:00:49.39	8.76*	8.66*	7.95±0.03	7.95±0.02	4.57± 0.10	-35.70	-13.10	5	08373381+2000492
11	8:37:36.33	19:15:53.96	14.05*	13.05*	10.76±0.02	10.34±0.09	0.51± 0.04	-35.30	-11.20	288	08373624+1915542
12	8:37:37.00	19:43:58.69	7.77*	7.79*	7.29±0.01	7.30±0.01	8.31± 0.09	N/A	N/A	6	08373699+1943585
13	8:37:40.71	19:31:06.38	8.29	8.20*	7.66±0.01	7.63±0.01	6.14± 0.08	-34.80	-12.50	10	08374070+1931063
14	8:37:42.36	19:08:01.57	10.05*	9.75*	8.58±0.02	8.58±0.02	2.57± 0.05	-36.60	-13.50	12	08374235+1908015
15	8:37:46.35	19:35:57.26	12.75	12.04	10.24±0.02	10.14±0.06	0.61± 0.03	-37.80	-9.40	295	08374640+1935575
16	8:37:46.64	19:26:18.10	10.85*	10.50	9.28±0.02	9.32±0.04	1.29± 0.04	-36.10	-13.40	13	08374660+1926181
17	8:37:46.77	19:16:02.03	6.75*	6.76*	6.17±0.01	6.12±0.01	24.79± 0.26	N/A	N/A	14	08374675+1916020
18	8:37:47.30	19:06:24.01	12.71	11.96*	10.20±0.02	10.07±0.07	0.65± 0.04	-35.60	-15.10	299	08374739+1906247
19	8:37:49.99	19:53:28.75	11.78*	11.13	9.33±0.02	9.10±0.04	1.59± 0.05	-31.80	-19.20	304	08374998+1953287
20	8:37:52.08	19:59:13.85	11.54	11.07	9.69±0.02	9.55±0.04	1.05± 0.04	-38.80	-14.60	310	08375208+1959138
21	8:37:57.06	19:14:09.67	12.23	11.59	10.04±0.02	10.11±0.09	0.63± 0.05	-35.40	-13.70	325	08375703+1914103
22	8:38:07.63	19:59:16.40	12.48	11.82	9.90±0.02	10.02±0.07	0.68± 0.05	-38.10	-13.50	346	08380758+1959163
23	8:38:08.08	20:26:20.83	12.08*	11.47*	9.93±0.02	10.03±0.17	0.68± 0.11	-36.40	-14.40	347	08380808+2026223
24	8:38:14.11	19:47:23.82	15.56	14.17	10.91±0.04	10.00±0.13	0.69± 0.08	N/A	N/A	358	08381421+1947234
25	8:38:14.28	19:21:55.37	11.20	10.31	9.19±0.02	9.12±0.03	1.56± 0.05	-35.00	-13.70	21	08381427+1921552
26	8:38:23.16	20:12:26.60	8.01*	7.71*	6.65±0.01	6.64±0.01	15.37± 0.13	N/A	N/A	-	08382311+2012263
27	8:38:24.31	20:06:21.92	10.80	10.40	9.18±0.02	9.23±0.03	1.41± 0.04	-36.30	-13.10	24	08382429+2006217
28	8:38:29.70	19:51:45.83	14.67*	13.53	10.93±0.02	10.56±0.14	0.41± 0.06	-40.10	-13.20	27	08382963+1951450
29	8:38:32.18	19:27:55.04	10.46*	9.65	7.54±0.01	7.46±0.01	7.18± 0.08	N/A	N/A	-	08383216+1927548
30	8:38:34.27	19:51:36.90	9.68	8.87	6.69±0.01	6.66±0.01	15.03± 0.18	N/A	N/A	-	08383425+1951369
31	8:38:37.43	19:01:14.81	14.45	13.27	10.61±0.01	10.16±0.18	0.60± 0.10	-37.70	-6.80	394	08383723+1901161
32	8:38:37.78	19:38:47.69	10.73*	10.43	9.22±0.02	9.24±0.05	1.40± 0.06	N/A	N/A	-	08383776+1938480
33	8:38:37.88	19:59:23.14	8.16*	8.16*	7.61±0.01	7.64±0.02	6.08± 0.08	-37.40	-13.60	35	08383786+1959231
34	8:38:46.97	19:30:03.53	9.08	8.95	8.22±0.02	8.08±0.02	4.06± 0.06	-34.80	-12.60	37	08384695+1930033
35	8:38:50.05	20:04:03.29	11.01	10.64	9.37±0.02	9.28±0.03	1.35± 0.03	-36.60	-15.40	423	08385001+2004035
36	8:38:53.57	19:34:17.90	14.82*	13.53*	10.96±0.02	10.92±0.17	0.30± 0.05	-40.90	-21.30	432	08385354+1934170
37	8:38:55.07	19:11:54.02	10.84	9.87	8.04±0.01	7.90±0.02	4.81± 0.08	N/A	N/A	-	08385506+1911539
38	8:39:01.89	20:00:19.62	12.48*	11.45*	9.07±0.02	8.96±0.03	1.80± 0.05	N/A	N/A	-	08390185+2000194
39	8:39:02.27	19:19:35.36	12.83	12.06	10.26±0.02	10.20±0.08	0.57± 0.04	-36.60	-10.50	448	08390228+1919343
40	8:39:02.84	19:43:28.99	9.48	9.19*	8.12±0.01	8.08±0.02	4.06± 0.06	-35.80	-11.20	46	08390283+1943289
41	8:39:03.24	20:02:35.12	15.18	13.86	11.05±0.02	10.88±0.13	0.31± 0.04	-40.70	-14.30	47	08390321+2002376
42	8:39:03.60	19:59:59.24	8.33*	8.32*	7.77±0.01	7.71±0.02	5.69± 0.09	-34.20	-13.30	48	08390359+1959591
43	8:39:04.09	19:31:23.20	14.40	13.28	10.86±0.01	10.46±0.13	0.45± 0.05	-37.00	-14.60	450	08390411+1931216
44	8:39:05.25	20:07:01.92	9.51	9.31*	8.41±0.02	8.38±0.03	3.09± 0.07	-35.70	-12.10	49	08390523+2007018
45	8:39:06.12	19:40:36.59	7.48*	7.43*	6.71±0.01	6.73±0.01	14.03± 0.17	N/A	N/A	50	08390612+1940364
46	8:39:06.55	19:00:36.68	13.83	13.09	11.30±0.02	11.16±0.30	0.24± 0.07	N/A	N/A	457	08390649+1900360
47	8:39:09.11	19:35:32.68	8.54*	8.49*	7.88±0.02	7.87±0.03	4.93± 0.12	-35.30	-12.00	52	08390909+1935327
48	8:39:10.15	19:40:42.56	9.55*	9.32*	8.41±0.01	8.40±0.02	3.03± 0.04	-36.10	-13.70	54	08391014+1940423
49	8:39:12.20	19:06:56.45	10.86	10.41	9.26±0.02	9.18±0.05	1.47± 0.07	-37.00	-13.40	57	08391217+1906561
50	8:39:15.05	20:12:39.35	11.61	11.13	9.65±0.02	9.63±0.06	0.97± 0.05	-35.20	-14.70	477	08391499+2012388
51	8:39:19.77	20:03:10.91	9.78	8.97	7.08±0.01	7.02±0.01	10.80± 0.14	N/A	N/A	-	08391972+2003107
52	8:39:21.88	19:51:40.86	12.97*	12.20	10.37±0.02	10.07±0.10	0.65± 0.06	-36.40	-8.80	65	08392185+1951402
53	8:39:24.99	19:27:33.70	10.75	10.01	9.00±0.01	8.89±0.03	1.92± 0.04	-37.00	-14.90	66	08392498+1927336

TABLE 1 — *Continued*

#	α_{2000} [h:m:s]	δ_{2000} [°:′:″]	g* [mag]	r* [mag]	K_{2MASS} [mag]	$[24]^{\dagger}$ [mag]	$F_{24}^{\dagger}$ [mJy]	μ_{α} [mas yr^{-1}]	μ_{δ} [mas yr^{-1}]	W#‡	2MASS
54	8:39:28.63	19:28:25.00	12.07*	11.32*	9.53±0.02	9.40±0.05	1.21± 0.06	-36.10	-10.80	506	08392858+1928251
55	8:39:29.42	19:47:11.51	13.09*	12.29	10.06±0.01	9.94±0.22	0.73± 0.14	-38.90	-9.00	69	08392940+1947118
56	8:39:30.44	20:04:08.69	10.68*	10.11	8.81±0.01	8.74±0.02	2.22± 0.03	-35.80	-13.40	70	08393042+2004087
57	8:39:33.44	20:10:10.52	9.79	8.67	6.13±0.01	6.00±0.02	27.56± 0.38	N/A	N/A	-	08393342+2010102
58	8:39:36.35	19:15:39.67	15.10*	13.87	11.01±0.02	10.49±0.12	0.44± 0.05	-33.30	-24.60	523	08393643+1915378
59	8:39:38.29	19:26:26.02	13.13	12.28	10.29±0.02	10.22±0.09	0.57± 0.04	-33.00	-9.60	77	08393836+1926272
60	8:39:42.66	19:46:42.49	6.69*	6.65*	6.00±0.01	5.98±0.01	28.02± 0.37	N/A	N/A	79	08394265+1946425
61	8:39:42.81	20:05:10.46	7.75*	7.73*	7.16±0.01	7.16±0.03	9.47± 0.23	N/A	N/A	80	08394279+2005103
62	8:39:43.35	19:25:10.52	12.27	10.86	7.90±0.02	7.76±0.01	5.44± 0.06	N/A	N/A	-	08394333+1925121
63	8:39:44.68	19:16:30.94	7.68*	7.69*	7.09±10.00	7.15±0.01	9.53± 0.10	N/A	N/A	82	08394466+1916308
64	8:39:45.78	19:22:01.06	10.93	10.50	9.26±0.02	9.39±0.04	1.21± 0.05	-35.40	-12.80	83	08394575+1922011
65	8:39:50.74	19:32:26.92	7.06*	6.26*	4.39±0.04	4.32±0.01	129.25± 1.24	N/A	N/A	86	08395072+1932269
66	8:39:50.86	19:33:02.23	12.15*	11.56*	10.00±0.02	9.77±0.06	0.86± 0.05	-36.10	-13.90	87	08395084+1933020
67	8:39:52.35	19:18:45.61	10.68	10.07	9.01±0.02	8.90±0.03	1.91± 0.05	-34.80	-14.30	89	08395234+1918455
68	8:39:55.08	20:03:54.47	10.37	10.02	8.96±0.02	8.86±0.04	1.99± 0.07	-37.50	-13.90	93	08395506+2003541
69	8:39:56.51	19:33:10.91	7.32*	7.33*	6.79±0.01	6.82±0.01	12.99± 0.15	N/A	N/A	94	08395649+1933107
70	8:39:57.78	19:32:29.26	7.58*	7.53*	7.01±0.02	7.01±0.01	10.84± 0.09	N/A	N/A	96	08395777+1932293
71	8:39:58.09	19:12:05.98	9.71	9.38	8.48±0.02	8.36±0.02	3.15± 0.07	-37.40	-12.50	97	08395807+1912058
72	8:39:58.40	20:09:29.99	8.71	8.86	8.10±0.01	8.03±0.07	4.26± 0.28	-36.00	-13.80	98	08395838+2009298
73	8:39:59.10	20:01:53.15	9.35	9.15	8.21±0.02	8.22±0.01	3.56± 0.05	-36.40	-16.20	99	08395908+2001532
74	8:39:59.19	19:40:08.58	9.86	9.69	8.78±0.02	8.73±0.03	2.24± 0.06	N/A	N/A	-	08395915+1940083
75	8:39:59.58	18:56:35.30	10.08*	9.95	9.30±0.01	9.32±0.05	1.29± 0.06	N/A	N/A	-	08395957+1856357
76	8:39:59.84	number19:34:00.55	12.41*	11.57*	9.48±0.02	9.31±0.04	1.31± 0.05	-33.80	-12.20	565	08395983+1934003
77	8:40:00.01	19:34:39.86	13.35*	12.51*	10.55±0.02	10.20±0.06	0.57± 0.03	-39.40	-4.20	100	08395998+1934405
78	8:40:00.64	19:48:23.44	10.49*	10.17*	9.08±0.02	8.97±0.03	1.80± 0.05	-36.30	-13.10	101	08400062+1948235
79	8:40:01.32	20:08:08.38	9.82*	9.57*	8.62±0.01	8.53±0.02	2.67± 0.05	-36.00	-14.50	102	08400130+2008082
80	8:40:01.72	18:59:59.17	10.47	9.93	8.70±0.02	8.48±0.03	2.81± 0.07	-36.50	-11.70	103	08400171+1859595
81	8:40:04.20	19:47:04.24	12.11	11.54	10.00±0.02	10.05±0.10	0.66± 0.06	-33.00	-13.70	576	08400416+1947039
82	8:40:04.92	19:43:45.48	9.95	9.67	8.65±0.02	8.54±0.03	2.65± 0.06	-36.10	-12.50	106	08400491+1943452
83	8:40:05.70	19:01:30.18	13.20	12.31	10.01±0.02	9.90±0.07	0.76± 0.05	-35.70	-12.20	578	08400571+1901307
84	8:40:06.28	19:27:14.80	10.55	10.10	8.87±0.02	8.80±0.03	2.10± 0.05	N/A	N/A	-	08400627+1927148
85	8:40:06.37	19:18:26.46	11.58*	10.76	9.23±0.02	9.23±0.03	1.40± 0.04	-34.30	-14.70	582	08400635+1918264
86	8:40:06.44	20:00:28.12	6.88*	6.06*	4.20±0.02	4.13±0.01	153.97± 1.35	N/A	N/A	111	08400643+2000280
87	8:40:09.74	19:37:17.83	12.54*	11.71	10.13±0.02	10.04±0.08	0.67± 0.05	-33.90	-10.50	114	08400968+1937170
88	8:40:11.46	19:58:16.21	6.78*	6.71	6.53±0.02	6.56±0.01	16.42± 0.17	N/A	N/A	115	08401145+1958161
89	8:40:12.32	19:38:22.78	10.07*	9.79*	8.67±0.02	8.56±0.03	2.62± 0.07	-36.90	-14.50	116	08401231+1938222
90	8:40:13.45	19:46:45.08	13.75*	12.79*	10.64±0.02	10.75±0.13	0.35± 0.04	-31.50	-14.40	117	08401345+1946436
91	8:40:15.36	19:59:39.66	8.88*	8.77*	8.04±9.99	8.03±0.02	4.27± 0.06	-35.80	-12.30	119	08401535+1959394
92	8:40:15.59	19:27:29.84	14.61	13.47	10.69±0.02	10.52±0.12	0.43± 0.05	-36.30	-8.50	601	08401549+1927310
93	8:40:15.72	19:54:54.07	13.15	12.29	10.01±0.02	9.92±0.06	0.75± 0.04	-38.00	-13.20	120	08401571+1954542
94	8:40:17.63	19:47:15.14	10.20	9.73*	8.58±0.02	8.60±0.03	2.52± 0.07	-35.50	-13.60	122	08401762+1947152
95	8:40:18.10	19:31:55.13	7.52*	7.57*	7.16±0.01	7.18±0.01	9.34± 0.08	N/A	N/A	123	08401810+1931552
96	8:40:18.97	20:11:31.16	13.59	12.38*	10.04±0.01	9.71±0.06	0.90± 0.05	-37.40	-14.00	607	08401893+2011307
97	8:40:20.16	19:20:56.44	6.83*	6.77*	6.04±0.01	6.01±0.01	27.23± 0.31	N/A	N/A	125	08402013+1920564
98	8:40:20.75	19:41:12.23	7.68*	7.69*	7.28±0.02	7.30±0.01	8.36± 0.11	N/A	N/A	127	08402075+1941120
99	8:40:22.09	19:40:11.82	6.95*	6.08*	4.18±0.03	4.07±0.01	162.87± 1.71	N/A	N/A	128	08402209+1940116
100	8:40:22.33	20:06:24.88	10.26	9.97	8.85±0.01	8.64±0.03	2.43± 0.06	-36.60	-12.20	129	08402231+2006243
101	8:40:22.73	19:27:53.46	10.94*	10.53*	9.34±0.02	9.25±0.04	1.39± 0.05	-37.80	-13.30	131	08402271+1927531
102	8:40:23.29	19:40:23.95	10.61*	10.20*	9.01±0.02	9.01±0.03	1.73± 0.04	-37.00	-11.80	132	08402327+1940236
103	8:40:23.48	19:50:06.04	8.09*	8.04	7.59±0.01	7.55±0.02	6.65± 0.10	N/A	N/A	133	08402347+1950059
104	8:40:25.55	19:28:32.92	9.75	9.37	8.76±0.02	8.71±0.03	2.28± 0.06	-36.80	-13.30	134	08402554+1928328
105	8:40:26.14	19:41:11.33	9.50*	9.27*	8.37±0.02	8.28±0.02	3.37± 0.05	-37.20	-11.90	135	08402614+1941111
106	8:40:26.30	19:13:11.06	13.40	12.50	10.46±0.02	10.56±0.13	0.42± 0.05	-38.40	-7.00	624	08402624+1913099
107	8:40:26.76	20:10:55.34	8.27*	8.17*	7.43±0.01	7.38±0.01	7.73± 0.09	N/A	N/A	136	08402675+2010552
108	8:40:27.03	19:32:41.42	6.27*	6.31*	5.88±0.01	5.92±0.01	29.83± 0.29	N/A	N/A	137	08402702+1932415

TABLE 1 — *Continued*

#	α_{2000} [h:m:s]	δ_{2000} [°:′:″]	g* [mag]	r* [mag]	K_{2MASS} [mag]	$[24]^{\dagger}$ [mag]	$F_{24}^{\dagger}$ [mJy]	μ_{α} [mas yr^{-1}]	μ_{δ} [mas yr^{-1}]	W#‡	2MASS
109	8:40:27.46	19:16:40.87	11.45	10.96*	9.65±0.02	9.58±0.04	1.02± 0.04	-33.30	-12.10	628	08402743+1916409
110	8:40:27.52	19:39:20.05	13.77*	12.83	10.69±0.02	10.84±0.12	0.32± 0.04	-33.40	-12.20	138	08402751+1939197
111	8:40:28.68	20:18:44.86	12.04*	11.35	9.46±0.02	9.42±0.07	1.18± 0.07	-37.40	-15.90	631	08402863+2018449
112	8:40:31.72	19:51:01.84	11.98*	11.38*	9.91±0.02	9.72±0.09	0.90± 0.07	-35.60	-12.90	640	08403169+1951010
113	8:40:31.85	20:12:5.98	11.85*	11.28	9.83±0.01	9.81±0.06	0.83± 0.04	-36.40	-13.90	641	08403184+2012060
114	8:40:32.97	19:11:39.59	8.72	8.55*	7.96±0.00	7.82±0.02	5.16± 0.10	-37.40	-14.20	141	08403296+1911395
115	8:40:33.48	19:38:00.42	12.63*	11.91*	10.17±0.02	10.05±0.08	0.66± 0.05	-38.90	-10.60	142	08403347+1938009
116	8:40:39.25	19:13:41.88	7.82*	7.80*	7.23±0.01	7.25±0.01	8.73± 0.10	N/A	N/A	150	08403924+1913418
117	8:40:39.94	19:40:09.37	11.44*	10.66	9.19±0.02	9.18±0.03	1.47± 0.05	-35.50	-11.30	151	08403992+1940092
118	8:40:41.91	19:13:25.68	10.86*	10.43*	9.06±0.02	9.04±0.03	1.68± 0.04	-35.90	-13.00	153	08404189+1913255
119	8:40:42.51	19:33:57.85	11.66*	11.11*	9.71±0.02	9.69±0.04	0.92± 0.04	-36.70	-13.80	154	08404248+1933576
120	8:40:43.22	19:43:09.62	7.07*	6.85	6.33±0.01	6.33±0.01	20.45± 0.14	N/A	N/A	156	08404321+1943095
121	8:40:46.09	19:18:34.67	9.79	9.45	8.53±0.02	8.49±0.02	2.79± 0.05	-37.10	-13.20	158	08404608+1918346
122	8:40:47.23	19:32:37.64	10.87	10.08	8.20±0.01	8.10±0.01	3.99± 0.05	N/A	N/A	-	08404720+1932373
123	8:40:48.01	19:39:31.57	11.56	10.79	9.25±0.02	9.25±0.03	1.39± 0.04	-37.60	-14.50	161	08404798+1939321
124	8:40:48.32	19:55:19.02	11.29	10.86	9.51±0.02	9.50±0.04	1.10± 0.04	-35.50	-13.00	162	08404832+1955189
125	8:40:52.52	20:15:59.87	8.52	8.47*	7.80±0.01	7.78±0.02	5.36± 0.08	-34.60	-12.70	166	08405247+2015594
126	8:40:52.53	19:28:59.77	10.55	10.15	9.05±0.02	8.97±0.03	1.79± 0.05	-37.00	-13.20	167	08405252+1928595
127	8:40:54.93	19:56:06.25	12.50*	11.80*	10.13±0.02	10.16±0.09	0.60± 0.05	-37.20	-14.90	677	08405487+1956067
128	8:40:56.29	19:34:49.26	6.76*	6.79*	6.28±0.01	6.28±0.01	21.23± 0.28	N/A	N/A	170	08405630+1934492
129	8:40:56.76	19:44:05.50	12.64*	11.94*	10.21±0.02	10.13±0.11	0.61± 0.06	-36.10	-11.10	171	08405669+1944052
130	8:40:56.95	19:56:05.57	8.79*	8.67*	8.05±0.02	7.95±0.01	4.57± 0.06	-36.10	-15.40	172	08405693+1956055
131	8:41:04.79	19:31:22.94	11.35	10.60	8.75±0.02	8.68±0.03	2.33± 0.06	N/A	N/A	-	08410478+1931225
132	8:41:07.34	19:26:48.08	13.01	12.12	10.29±0.02	10.30±0.20	0.53± 0.09	-43.70	-8.10	176	08410725+1926489
133	8:41:07.39	19:04:16.43	10.56	10.04	8.64±0.02	8.53±0.03	2.68± 0.06	-39.90	-14.10	177	08410737+1904164
134	8:41:09.61	19:51:18.32	11.01*	10.50*	8.94±0.02	8.61±0.03	2.48± 0.06	-36.70	-13.90	179	08410961+1951186
135	8:41:09.82	19:56:07.04	14.26*	13.19	10.76±0.02	10.67±0.10	0.37± 0.04	-42.40	-15.10	180	08410979+1956072
136	8:41:10.02	19:30:32.18	10.35*	9.98	8.91±0.02	8.83±0.13	2.04± 0.23	-36.90	-12.00	182	08411002+1930322
137	8:41:10.32	19:49:07.10	11.84*	11.29*	9.75±0.02	9.62±0.05	0.98± 0.04	-36.50	-13.20	183	08411031+1949071
138	8:41:10.70	19:49:46.38	9.06	8.86	8.19±0.01	8.19±0.02	3.66± 0.06	-37.80	-13.70	184	08411067+1949465
139	8:41:13.04	19:32:34.26	15.06	13.73	10.35±0.02	10.22±0.08	0.56± 0.05	-37.60	-9.70	709	08411319+1932349
140	8:41:13.80	19:55:19.24	8.35*	8.35*	7.77±0.01	7.69±0.02	5.82± 0.09	-36.90	-12.60	188	08411377+1955191
141	8:41:15.43	20:02:15.04	14.99*	13.78*	11.02±0.02	10.79±0.11	0.34± 0.03	-37.30	-11.90	189	08411541+2002160
142	8:41:16.04	19:44:54.13	14.06	13.44	11.71±0.02	10.50±0.09	0.44± 0.03	N/A	N/A	190	08411602+1944514
143	8:41:18.42	19:15:39.38	7.95*	7.90*	7.29±0.02	7.04±0.01	10.61± 0.12	-37.40	-12.90	192	08411840+1915394
144	8:41:19.96	19:38:04.20	14.20	13.09	10.76±0.02	10.22±0.17	0.56± 0.09	-36.30	-12.00	721	08411992+1938047
145	8:41:22.48	18:56:00.17	13.49	12.60	10.54±0.02	10.20±0.15	0.58± 0.08	-34.00	-9.90	726	08412258+1856020
146	8:41:23.93	20:14:57.30	15.46*	14.11*	10.78±0.02	10.11±0.13	0.63± 0.08	N/A	N/A	194	08412390+2014572
147	8:41:25.89	19:56:36.85	10.92*	10.55	9.33±0.02	9.37±0.04	1.24± 0.05	-36.30	-13.70	195	08412584+1956369
148	8:41:26.98	19:32:32.71	10.05	9.73*	8.72±0.02	8.79±0.03	2.12± 0.06	-37.30	-12.40	196	08412698+1932329
149	8:41:28.65	19:44:49.13	11.43	10.76	9.47±0.02	9.44±0.13	1.16± 0.14	-39.00	-13.50	198	08412869+1944481
150	8:41:33.89	19:58:08.83	12.07	11.47*	9.93±0.01	9.94±0.07	0.73± 0.05	-39.40	-14.40	201	08413384+1958087
151	8:41:35.09	19:39:45.04	9.17*	8.12	5.96±0.02	5.86±0.01	31.26± 0.30	N/A	N/A	-	08413506+1939449
152	8:41:35.90	19:06:25.16	14.84	13.59	10.98±0.02	10.55±0.11	0.42± 0.04	-31.10	-9.60	751	08413599+1906255
153	8:41:36.20	19:08:33.58	9.57	9.23	8.35±0.02	8.34±0.02	3.21± 0.05	-36.00	-14.30	204	08413620+1908335
154	8:41:37.43	19:31:13.08	14.19	13.09	10.73±0.01	10.50±0.14	0.44± 0.06	-40.90	-12.00	758	08413741+1931140
155	8:41:42.31	19:39:37.98	9.72*	9.50*	8.48±0.02	8.38±0.03	3.09± 0.08	-37.30	-13.80	206	08414229+1939379
156	8:41:43.68	19:57:43.85	12.73	12.05	10.26±0.02	10.15±0.10	0.60± 0.10	-40.50	-13.10	769	08414368+1957437
157	8:41:43.85	20:13:37.06	10.69	10.34	9.14±0.01	8.99±0.04	1.76± 0.07	-37.40	-15.70	771	08414382+2013368
158	8:41:45.49	19:16:02.17	10.35	9.98*	8.93±0.02	8.92±0.03	1.88± 0.05	-38.10	-13.20	208	08414549+1916023
159	8:41:47.74	19:24:43.88	11.66*	11.28	10.10±0.02	9.96±0.07	0.72± 0.05	-30.30	-9.50	-	08414776+1924439
160	8:41:48.24	19:27:30.49	14.28*	13.24	10.73±0.01	10.62±0.10	0.39± 0.04	-40.80	-9.80	774	08414818+1927312
161	8:41:49.34	19:11:47.51	15.24	13.90	10.83±0.01	10.55±0.11	0.42± 0.04	-33.90	-10.80	776	08414934+1911471
162	8:41:50.09	19:52:27.19	7.37*	6.56*	4.68±0.00	4.63±0.01	97.51± 1.02	N/A	N/A	212	08415008+1952270
163	8:41:51.98	20:10:01.99	12.44*	11.76*	10.09±0.02	9.78±0.08	0.85± 0.07	-40.60	-15.70	213	08415199+2010013

Gáspár et al.

TABLE 1 — *Continued*

#	α_{2000} [h:m:s]	δ_{2000} [°:′:″]	g* [mag]	r* [mag]	K_{2MASS} [mag]	[24][†] [mag]	F_{24}[†] [mJy]	μ_α [mas yr^{-1}]	μ_δ [mas yr^{-1}]	W#[‡]	2MASS
164	8:41:53.16	20:09:34.16	8.61*	8.51*	7.79±0.01	7.71±0.01	5.71± 0.07	-38.20	-13.70	214	08415314+2009340
165	8:41:54.37	19:15:27.14	11.65	11.03	9.64±0.02	9.56±0.05	1.04± 0.05	-34.80	-13.20	215	08415437+1915266
166	8:41:55.90	19:41:22.96	11.39	10.86	9.54±0.01	9.59±0.07	1.02± 0.07	-37.60	-12.10	217	08415587+1941229
167	8:41:57.84	18:54:42.08	9.66*	9.35	8.43±0.02	8.43±0.03	2.94± 0.07	-34.30	-11.10	218	08415782+1854422
168	8:41:58.86	20:06:26.82	13.77*	12.83	10.60±0.01	10.32±0.16	0.52± 0.08	-40.30	-11.80	792	08415884+2006272
169	8:42:05.50	19:35:57.95	11.07	10.33*	8.38±0.03	8.30±0.02	3.32± 0.05	N/A	N/A	-	08420547+1935585
170	8:42:06.51	19:24:40.72	7.96*	7.97*	7.43±0.01	7.39±0.01	7.64± 0.06	-38.40	-12.10	223	08420650+1924405
171	8:42:10.79	18:56:03.62	7.92*	7.93*	7.35±0.01	7.35±0.02	7.95± 0.11	-34.10	-12.10	224	08421080+1856037
172	8:42:11.50	19:16:36.37	12.57*	11.85*	10.17±0.01	9.99±0.06	0.70± 0.04	-37.60	-10.00	817	08421149+1916373
173	8:42:12.34	19:12:48.20	14.32	13.20	10.83±0.01	10.56±0.10	0.41± 0.04	-33.50	-9.60	822	08421233+1912488
174	8:42:12.85	19:16:03.79	14.10*	13.07	10.48±0.01	10.11±0.06	0.63± 0.04	-33.00	-11.70	824	08421285+1916040
175	8:42:15.50	19:41:15.47	10.12	9.78	8.77±0.01	8.72±0.02	2.24± 0.05	-37.60	-15.00	226	08421549+1941156
176	8:42:18.85	20:24:36.22	12.59	11.91	10.19±0.02	10.05±0.12	0.66± 0.08	N/A	N/A	839	08421883+2024350
177	8:42:20.16	20:02:11.72	9.91	9.56	8.41±0.02	8.40±0.02	3.03± 0.06	-35.70	-15.60	228	08422012+2002117
178	8:42:21.62	20:10:53.72	9.32	9.13	8.28±0.01	8.13±0.02	3.89± 0.06	-36.80	-14.40	229	08422162+2010539
179	8:42:24.74	19:35:17.27	11.21	10.83*	9.48±0.01	9.34±0.04	1.27± 0.05	N/A	N/A	-	08422471+1935175
180	8:42:32.27	19:23:46.25	11.38	10.84	9.46±0.01	9.50±0.06	1.10± 0.06	-36.50	-12.50	232	08423225+1923463
181	8:42:40.19	19:07:58.87	12.55*	11.86*	10.19±0.01	9.83±0.06	0.81± 0.04	-35.30	-10.90	863	08424021+1907590
182	8:42:40.73	19:32:35.34	10.03	9.66	8.72±0.02	8.67±0.03	2.36± 0.07	-38.40	-12.70	235	08424071+1932354
183	8:42:42.51	19:05:59.78	12.04*	11.38	9.88±0.02	9.88±0.06	0.78± 0.04	-37.40	-13.50	236	08424250+1905589
184	8:42:43.72	19:37:23.52	12.76	11.76	9.80±0.02	9.64±0.05	0.97± 0.04	-36.40	-14.20	868	08424372+1937234
185	8:42:44.44	19:34:48.11	10.09	9.53	8.63±0.02	8.48±0.02	2.82± 0.05	-38.20	-13.50	238	08424441+1934479
186	8:43:00.59	20:20:15.79	11.76	11.24	9.77±0.02	9.57±0.06	1.03± 0.06	-37.30	-16.00	887	08430055+2020161
187	8:43:05.96	19:26:15.36	10.25	9.65	8.46±0.02	8.40±0.01	3.02± 0.04	-36.60	-13.80	248	08430593+1926152
188	8:43:08.24	19:42:47.59	13.92	12.89	10.67±0.01	10.15±0.09	0.60± 0.05	-33.70	-11.60	899	08430822+1942475
189	8:43:10.82	19:31:33.64	12.20	11.58	10.01±0.02	10.49±0.22	0.44± 0.09	-38.50	-17.50	902	08431076+1931346
190	8:43:20.20	19:46:08.58	11.05	10.62	9.36±0.02	9.26±0.04	1.37± 0.05	-39.40	-13.40	255	08432019+1946086
191	8:43:32.42	19:44:38.00	12.92	12.01	10.22±0.02	9.94±0.08	0.73± 0.05	-40.10	-16.50	919	08433239+1944378
192	8:43:35.56	20:11:22.63	10.29	9.99	8.92±0.02	8.95±0.03	1.82± 0.05	-39.30	-14.70	257	08433553+2011225
193	8:44:07.37	20:04:36.23	10.30	10.05	9.06±0.01	8.95±0.03	1.82± 0.04	N/A	N/A	-	08440734+2004369

* The r and/or g magnitudes marked with a star were calculated from B and V magnitudes as described in §3, while the rest are the original SDSS values.

† The [24] magnitudes are the ones that were calibrated to the 2MASS K_S magnitudes, while the mJy values in the F_{24} column are the original flux values.

‡ The numbers in this column represent the numbering of Wang et al. (1995).